Bachelor Project

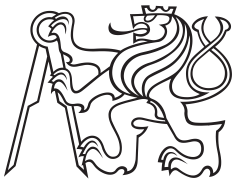

Czech Technical University in Prague

F3

Faculty of Electrical Engineering
Department of Circuit Theory

Educational Simulator of Glucose Metabolism in a Web Browser

Ondřej Skrla

Supervisor: doc. MUDr. Jiří Kofránek, CSc.
2023

BACHELOR'S THESIS ASSIGNMENT

I. Personal and study details

Student's name: **Skrla Ondřej** Personal ID number: **492111**

Faculty / Institute: **Faculty of Electrical Engineering**

Department / Institute: **Department of Circuit Theory**

Study program: **Medical Electronics and Bioinformatics**

II. Bachelor's thesis details

Bachelor's thesis title in English:

Educational simulator of glucose metabolism in a web browser

Bachelor's thesis title in Czech:

Výukový simulátor glukózové regulace v internetovém prohlížeči

Guidelines:

Develop an educational glucose regulation simulator combining a simulation model with web graphics and hypertext. Review mathematical models of glucose metabolism and create a mathematical model of glucose metabolism. Design the structure of a tutorial page for a glucose and insulin simulator.Use the Bodylight.js technology (https://bodylight.physiome.cz/) to create the web simulator, and use the Modelica language development environment - (https://openmodelica.org/) to develop the model.

Bibliography / sources:

[1] SORENSEN, John Thomas. A physiologic model of glucose metabolism in man and its use to design and assess improved insulin therapies for diabetes. PhD diss., Massachusetts Institute of Technology, 1985. [2] PRATT, Adrian C., Jonathan A. D. WATTIS, and Andrew M. SALTER. Mathematical modelling of hepatic lipid metabolism. Mathematical Biosciences [online]. 2015, 262, 167–181 [viewed 3 January 2023]. ISSN 0025-5564. Available from: doi:10.1016/j.mbs.2014.12.012 [3] WANG, ZiMian, et al. Specific metabolic rates of major organs and tissues across adulthood: evaluation by mechanistic model of resting energy expenditure. The American Journal of Clinical Nutrition[online]. 2010, 92(6), 1369–1377 [viewed 21 October 2022]. ISSN 1938-3207. Available from: doi:10.3945/ajcn.2010.29885

Name and workplace of bachelor's thesis supervisor:

doc. MUDr. Jiří Kofránek, CSc. Ústav patologické fyziologie, 1. LF UK Praha

Name and workplace of second bachelor's thesis supervisor or consultant:

Date of bachelor's thesis assignment: **10.01.2023** Deadline for bachelor thesis submission: **10.01.2023**

Assignment valid until: **10.01.2024**

doc. MUDr. Jiří Kofránek, CSc.	doc. Ing. Radoslav Bortel, Ph.D.	prof. Mgr. Petr Páta, Ph.D.
Supervisor's signature	Head of department's signature	Dean's signature

III. Assignment receipt

The student acknowledges that the bachelor's thesis is an individual work. The student must produce his thesis without the assistance of others, with the exception of provided consultations. Within the bachelor's thesis, the author must state the names of consultants and include a list of references.

. | Date of assignment receipt

Student's signature

Acknowledgements

I would like to thank my supervisor doc. MUDr. Jiří Kofránek, CSc. for allowing me to work on this topic and for his encouragement throughout working on the thesis. I would also like to thank Ing. Jan Havlík, PhD. for granting the thesis his auspices in the Department of Circuit Theory and his help with the submission process. Further I would like to thank Bc. Lucie Malánová for critically rereading the text and for making useful suggestions.

Declaration

I declare that this thesis has been composed solely by myself and that I have listed all used information sources in accordance with the Methodological Guideline on Ethical Principles of the Preparation of University Graduate Thesis.

Prohlašuji, že jsem předloženou práci vypracoval samostatně a že jsem uvedl veškeré použité informační zdroje v souladu s Metodickým pokynem o dodržování etických principů při přípravě vysokoškolských závěrečných prací.

Prague, January 10th, 2023

Ondřej Skrla

Abstract

This thesis develops a mathematical model of glucose metabolism and builds an educational web-page application where the user can explore different aspects of glucose metabolism through simulation. The model is built primarily on the work of T. J. Sorensen who proposed a whole-body glucose metabolism model in his 1985 dissertation thesis. Other models are adapted to and combined with the Sorensen's model to add intracellular dynamics to the model. After discussing the theory of glucose metabolism and the equations of the model, parameters are discussed and estimated. The model is implemented in Modelica using the object inheritance approach which enhances the model's adaptability. The model is tested through glucose and insulin infusion experiments and compared with experimental data. On the qualitative level, the results agree with the experimentally measured values. To produce the web page, an educational concept of showing specific points of view on glucose metabolism is proposed. Namely, closed loop of organs, cycling of metabolites, intracellular reactions, and regulation of homeostasis. Bodylight.js tools are used for the implementation of the web page.

Keywords: glucose metabolism, mathematical modeling, educational modeling, Modelica, T. J. Sorensen

Supervisor: doc. MUDr. Jiří Kofránek, CSc.

Abstrakt

Tato práce navrhuje matematický model metabolismu glukózy a vytváří výukovou webovou aplikaci, ve které může uživatel prostřednictvím simulace prozkoumat různé aspekty metabolismu glukózy. Model je postaven především na práci T. J. Sorensena, který ve své dizertační práci z roku 1985 navrhl model celotělového metabolismu glukózy. Pro popis vnitrobuněčných reakcí práce napojuje na Sorensonův model další modely. Po představení teorie metabolismu glukózy a rovnic modelu práce diskutuje odhad a výpočet parametrů modelu. Model je implementován v jazyce Modelica s využitím dědičnosti objektů, což ho činí snadněji použitelným pro další vývoj. Model je porovnán s experimentálními daty, se kterými je na kvalitativní úrovni v souladu. Struktura webové stránky je navržena tak, aby poskytla pohled na glukózový metabolismus z různých úhlů pohledu. Konkrétně pohled na orgány jako na uzavřenou smyčku, na cyklování metabolitů, na vnitrobuněčné reakce a na regulaci homeostázy. Pro implementaci webové stránky jsou použity nástroje Bodylight.js.

Klíčová slova: glukózový metabolismus, matematické modelování, modelování pro výuku, Modelica, T. J. Sorensen

Překlad názvu: Výukový simulátor glukózové regulace v internetovém prohlížeči

Contents

Figures

Tables

Chapter 1

Introduction

Human metabolism has many routes and systems highly important both in health and in disease - one of them being glucose metabolism. Changes in glucose metabolism can result in severe health complications, like diabetes mellitus of the second type which affects circa 6% of the global population. [46] Apart from type 2 diabetes, a range of other alternations exist to glucose metabolism since the human glucose metabolism is broad and complex. Its effects have no clear boundaries, affect nearly all tissues in the body, and are deeply connected to other metabolic cycles, for example, fatty acid or amino acid metabolism. Even the portion of glucose metabolism related to energetics is bounded to many other subsystems and is difficult to grasp as a whole. Hence understanding glucose metabolism is important, yet complicated. The human glucose metabolism can be observed in vivo or in vitro, but that is not always suitable since it often requires special expertise and tools and still captures only a section of the system as a whole. An alternative to that is to provide a more complex description of the system through text (with images and diagrams), but that usually carries with it low levels of adaptability and visualization potential. This issue represents an obstacle in education where students have to comprehend large systems before gaining practical experience. Therefore, the primary motivation of this thesis is to create a more accessible path to studying and understanding glucose metabolism.

Mathematical modeling is an approach that can make the studying of glucose metabolism more available. It can help test hypotheses, predict new therapies, or study the metabolism under conditions that would be difficult or impossible to produce in real life. That is why mathematical modeling is used as an approach to solving the objective of this thesis. However, glucose metabolism models available in the literature were mostly not developed for educational purposes, and using them might be nonfunctional. The models in the literature of glucose metabolism are usually developed with specific motivations; for example research of diseases and therapies. With that, they are often reduced to a minimal working system that can represent the studied disease. This makes their ability to be directly adapted to different scenarios limited - which is important in modeling for education. Furthermore, these models are not holistic and provide great detail in certain parts of the body, while neglecting others. Furthermore, mathematical models often require specific software and

certain technical knowledge to implement them, which might be difficult to access for the potential user. To benefit from the advantages of modeling in education, the objective of this thesis is to provide an educationally tailored model delivered on an accessible platform.

For the model, the goal is to offer a complete picture of the body with a similar level of depth of detail in different tissues. The aim is also to first show a complete typical metabolism and then change it flexibly to demonstrate its variations in disease. The approach is to build upon existing glucose metabolism models of T. J. Sorensen[80], Pratt et al.[71] and Carstensen et al.[14] and use them to create a whole-body model. This model will be displayed on a web page simulator. A web page represents a suitable platform for the model as it is accessible and there is an existing tool chain to convert models to interactive web page components. The combination of a model and a web page represents a good fit for education as it combines the interactivity of the web components with the model's capacity to visualize processes. To develop the model and construct the web page, OpenModelica environment, and Bodylight.js tools will be used.

The selected tissues to be modeled are the brain, liver, adipose tissue, heart, skeletal muscle, kidneys, and gut. The modeled tissues will contain intracellular processes which will drive the simulated metabolism. The model also will include hormonal regulation by insulin and glucagon. The model will simulate a standard 70 kg male glucose metabolism that can be altered to simulate glucose intolerance or decreased insulin production. How glucose metabolism behaves can rapidly change depending on the person's activity; in a fasted state, shortly after eating, or during exercise. The model will simulate a basal state after an overnight fast which can be altered by insulin or glucose infusions. Exercise or food intake will not be modeled.

1.1 State of the art

A very common way of modeling the metabolism of glucose and related metabolites is through ordinary differential equations (ODEs). This approach has been dominant throughout the last years [4] and models built on ODEs can be implemented in the language of Modelica in a straightforward way, for these reasons only ODE models will be considered.

1.1.1 Minimal models

One of the first widely cited models regarding energetic metabolism began to be formulated in the 70s and 80s as clinical tools for glucose measurements. The Bergman et al. model[9] aimed to estimate insulin sensitivity for clinical use by devising a 'minimal model' for use during an intravenous glucose tolerance test (IVGTT). The model contained two differential equations and considered liver and periphery interactions governed by glucose and insulin.[4] A variety of minimal models followed, for example, Silber et. al

(2007) produced a more detailed model using 15 equations describing the post-IVGTT differences between healthy and diabetic people. The model used several compartments but these were modeled less as organs and more as functional flows. [77] The response to oral glucose tolerance tests (OGTT) was also modeled by Silber et. al (2010) and followed a similar approach as in the 2007 paper. [78] A recent model in this line of research brought a more detailed description of insulin kinetics by including a pancreas compartment. [23] Following the success of the Bergman et al. minimal model, Derouich and Boutayeb edited the model to contain the effects of exercise, still described by two ODEs. [19] However, as the minimal models do not attempt to model multiple organs as compartments nor do they use more detailed chemistry, they are not a suitable choice for an educational model.

1.1.2 Whole-body models

Another motivation for the development of metabolic models was the creation of virtual diabetic patients and insulin delivery algorithm testing. The model of Dalla Man et al. became truly successful as it even became accepted by the United States of America Federal Drug Agency as a tool for pre-clinical diabetes technology trials. The original model consisted of glucose and insulin as mediators and contained both a healthy person and a diabetic person model. [18] Later updates included glucagon and focused on developing a type 1 diabetes mellitus (T1DM) virtual patient population and added tools for simulating subcutaneous insulin delivery and continuous glucose measurements. [92] There are also other commercial simulators that are not discussed here (T1DM PhysioLab, Archimedes).

More detailed kinetic processes of energetic metabolism were modeled for example by Liu and Tang who developed a more detailed metabolism model for algorithm testing, including glycogen mechanics in the liver and glucagon regulation. [54] Other works have focused on including other metabolites, such as free fatty acids, hence modeling the metabolism more as a whole. Xu et al. investigated the role of glycogen cycling in metabolism in the liver [94]. Both of these models have a larger amount of detail than the minimal models, however, Liu et al. split the body only into plasma and intracellular space, which is still very broad for the purposes of this thesis, and the work of Xu et al. omitted the kidneys and the brain from their model. Pratt et al. focused more on the dynamics of lipids but also modeled some glucose metabolites in the liver. [71] Both the Xu et al. and Pratt et al. models were structured into adipose tissue, muscle, liver, and blood plasma and didn't explicitly model any incretins effects. Only the Xu et al. model included glucagon explicitly.

The effect of oral glucose ingestion and the effect of incretins has been modeled for example by Toghaw et al. [83] Their model described glucose, insulin, incretin, and ghrelin dynamics and split the small intestine into three compartments. However, the main purpose of the model was the simulation of the effects of bariatric surgery, and less the simulation of general metabolism. Some more complex models were structured hierarchically. Nyman et al.

integrated a cell-level model of insulin-glucose mechanics in adipocytes into the model of Dalla Man et al. from 2007. [66] Later, the same research group made an extension to the model including adding a brain component, liver glucose intake after meals, and other effects. [36] A different branch of research by Uluseker et. al also extended the Nyman et al. model, focusing on enhancing the model with ghrelin, leptin, incretin, and glucagon. [85] A sophisticated model of a whole-body metabolism was constructed by Kurata, with over 200 metabolites described by differential equations spanning all major organs, including the brain. [49] While these models offer in-depth insight into intracellular processes, perhaps an unnecessary amount of detail for a general educational model is included. In the case of the Nyman et al. model and the subsequent models, the adipocyte module is very detailed while the rest is generally put. The work of Kurata is too complex to be simply visualized and would leave much of the model's mechanics unused.

A popular whole-body model was developed by Sorensen, based on blood flows between individual organs, including the brain, which isn't explicitly often accounted for. The modeled substances were glucose, insulin, and glucagon. [80] Recently, Panunzi et al. extended Sorensen's model to include a glucose digestion module and corrected its mistakes. [69] Building on the work of Sorensen, Alvehag, and Martin extended his model to include incretin dynamics, as a base model for type 2 diabetes mellitus (T2DM) modeling. [5] Alvehag and Martin's work was further developed and validated by Vahidi et al., who also focused on modeling the effects of incretin. [87] Schaller et al. followed the work of Sorensen and produced a whole-body system with great cellular detail. Each organ is divided into additional sub-compartments and molecular insulin signaling is modeled. In addition to the source model, incretin effects are also modeled. The model of Schaller et al. would be possibly suitable but no explicitly written equations were published in the paper. [74] Very recent pre-print conference paper by Carstensen et al. expanded the Sorensen model to simulate whole-body metabolism with 16 metabolites related to glucose, lipid, and also amino-acid cycles. [14]

1.2 Structure of the thesis

The thesis is divided into three sections - theory, implementation, and conclusion. In the Theory section, Sorensen's model is introduced and the biology of glucose metabolism is described, both from a whole-body and intracellular point of view. The software used for implementation is referenced. In the Implementation section, the parameters and equations of the model are discussed, and also the practical implementation in OpenModelica is explained. The discussion is divided into whole-body constants and then individual organs, following the approach of Sorensen. The model simulations are compared with data from the literature. The concept of the web page and how it's structured is discussed as the last part of the Implementation section. In the Conclusion section, the results of the thesis are reviewed, along with its limitations and further possible developments.

Chapter 2

Theory

This chapter describes the selected base model (Sorensen's model) and glucose metabolism on whole-body and intracellular levels. Glucose intolerance is introduced and finally, a short list of the used software tools is referenced.

2.1 Sorensen's model

When searching for a model to work with, the goal was to find a model containing both insulin and glucagon and most of the major body organs. The original model of Sorensen was selected as it provides an account of the whole body and can be expanded in a straightforward way because it uses common general principles across all modeled tissues and organs. The limitation of the model for the purposes of this thesis is the lack of intracellular reactions and the combination of muscle tissue and adipose tissue into one compartment. These will be solved in the section on implementation. In this subsection, two important concepts from the work of Sorensen are described; how metabolites circulate between organs and how to efficiently model the effects of hormones and other regulators.

2.1.1 Metabolite mass equations

The organs and tissues with which he works are brain, gut, liver, kidney, heart & lungs and periphery. Some organs have separate interstitium and vessels, some are simply combined into one space. A simple organ glucose mass equation is written

$$V\frac{dG^{out}}{dt} = Q^{inp}G^{inp} - Q^{out}G^{out} - r_{sink} + r_{source} \tag{2.1}$$

where V is the sum of the vessel and interstitium volumes, G is glucose concentration (input or output), Q is the blood flow (input or output), r are sinks and sources originating from processes in the tissue. The equations for separated compartments

$$V_V\frac{dG_V}{dt} = Q^{inp}G^{inp} - Q^{out}G_V - \frac{V_I}{T}(G_V - G_I) \tag{2.2}$$

$$V_I \frac{dG_I}{dt} = \frac{V_I}{T}(G_V - G_I) - r_{sink} + r_{source} \tag{2.3}$$

where the subscript V and I denotes vessels and interstitium and T is the membrane transport time constant. The two compartment model is used in scenarios where there is a steep concentration gradient (periphery block, brain).

Sorensen does not model intracellular processes as it is not necessary in his model and simply estimates the processes in the extracellular space. Insulin equations work similarly to the glucose mass equations. The glucagon module is considered to have a single mixed volume representing the whole body and does not circulate.

2.1.2 Estimation of sinks and sources

A key principle for Sorensen is that the effects of hormones (insulin, glucagon) and glucose are multiplicative and can be separated. For a metabolic sink or source, the rate r is expressed as:

$$r = M^I M^\Gamma M^G r_B \tag{2.4}$$

where M are the multiplier functions, depending only on *one* normalized (with respect to basal levels) metabolite concentration, and r_B is the basal rate of the sink/source. Sorensen modeled these M functions as tanh functions. An important feature of this set up is that M functions are always normalized, hence at basal state they equal to one and hence $r = r_B$; which is very elegant and practical. This approach is the corner stone of this thesis' model too.

Usually, Sorensen would first discuss and determine the basal rates. By using measurements from various studies, most of the time he was able to discern individual effects and fit on the study data tanh M functions by using the Levenberg-Marquardt optimization method. In cases where this was not possible (mainly the liver), the curves were fit to match data from intravenous glucose tolerance test (IVGTT). Similarly the pancreas release module was fit to the IVGTT data.

2.2 Glucose metabolism

2.2.1 Whole-body glucose metabolism

During the basal state when there has been no energy substrate intake for several hours, the body equilibrates and the endogenous glucose production matches the consumption. The main glucose-consuming organ is the brain with very limited fluctuation. In case of decreased blood glucose levels, the brain will always get prioritized. Another tissue that uptakes glucose in significant amounts is the muscle tissue, which, similarly to the heart, uses glucose only as a minor substrate. The adipose tissue has low energy

requirements but uses glucose as its main substrate. [25] Interestingly, the small intestine also clears a portion of glucose but not for energetic purposes but for the production of other substrates.[60] The liver and the kidney both uptake glucose for the production of energy, yet also have the capacity to produce glucose from other substrates or from storage in the case of the liver. Red blood cells and lungs[68] also uptake significant portions of glucose. Understanding the basal state is important as that will be the default state of the model.

After the consumption of a meal, the metabolism switches on multiple levels. In tissues where fatty acids were the dominant metabolic substrate, glucose is primarily utilized. Furthermore, in adipose tissue lipid breakdown is reduced and lipid storage is promoted together with glucose uptake. The liver nearly stops its glucose production and directs the incoming glucose toward storage as glycogen. The skeletal muscle also not only utilizes glucose but also stores it as glycogen. These processes are mediated by changes in insulin, glucagon, catecholamine, and other control hormone concentrations.[79] Even though meal ingestion reaction differs from simple glucose infusion reaction, the principle responses remains the same.

2.2.2 Reduced glucose tolerance

Reduction in glucose tolerance can be seen in higher than usual blood glucose levels or reduced glucose clearance during glucose infusion (or consumption). Glucose tolerance is considered in the context of type 1 and type 2 diabetes mellitus. Type 1 is characterized by the destruction of beta-cells which causes a diminished or absent response of insulin to increased blood glucose levels. Type 2 can have various forms, but generally includes both insulin resistance and modified insulin release. The tissues mainly involved in insulin resistance are skeletal muscles, adipose tissue, and the liver. The resistance in these tissues can have two parts - receptive and reactive. The receptive part concerns the availability of insulin receptors - if only receptivity is reduced, then a sufficient amount of insulin will achieve a similar response to a non-resistant tissue. The reactivity of tissue to insulin characterizes dysfunction in the insulin's signaling cascades. ([80], p. 305-335)[1] This could be caused, at least in type 2 diabetes, by inflammation and reactive oxygen species. In the adipose tissue, insulin resistance causes high lipolysis rates which impact the metabolism of other organs. In the liver, insulin resistance causes insufficient drive of glucose towards storage and does not inhibit the glucose-releasing pathways. [27] The conclusion from this section is that although the intracellular mechanisms leading to insulin resistance and beta-cell inactivity/death are complicated, in principle there are three general phenomena; insulin production, insulin receptivity, and insulin reaction; that are altered. This observation could be useful for designing the glucose

[1] The page numbers when referencing Sorensen are added even in cases which are not inline citations so that information could be more easily found since a wide range of pages is referenced from the thesis.

intolerant metabolism later on.

2.2.3 Glycolysis and gluconeogenesis

In the cell, glucose can undergo glycolysis, a process of converting glucose to pyruvate. Each step in the pathway is catalyzed by a specific enzyme. A key enzyme is a hexokinase which converts glucose to glucose-6-phosphate. The next step is catalyzed by phosphofructokinase-1 (PFK-1). After some additional steps, glyceraldehyde-3-phosphate (G3P) is created. The last step before pyruvate is created is the formation of phosphoenolpyruvate (PEP). Hexokinase has different forms, one of them being specifically called glucokinase, which is localized to the liver. After glycolysis, pyruvate can turn into lactate or acetyl co-enzyme A (ACoA). ACoA then enters the tricarboxylic acid cycle to undergo full oxidation. ACoA can also be used to create fatty acids. G3P can enter the fatty acid metabolism as glycerol-3-phosphate and become the backbone of a triglyceride. [53]

The formation of glucose from different substrates is termed gluconeogenesis. The most typical source substrates are lactate, amino acids, and glycerol. Depending on the substrate, the pathways differ in the beginning, but all essentially have to go through the tricarboxylic acid cycle before being converted to PEP. An important enzyme in this process is the phosphoenolpyruvate carboxylate kinase (PEPCK). Pyruvate by itself cannot be directly converted to PEP and has to pass through the mitochondria. The final step of conversion of glucose to G6P is catalyzed by the enzyme G6Pase. [98] These glycolytic and gluconeogenic paths form the basis of the intracellular scheme of reactions in the model. Furthermore, knowing the enzymatic breakpoints is necessary to correctly assign the insulin effects to the intracellular reactions they affect.

2.3 Tools for implementation

The model will be developed in the Modelica programming language. As the accessibility of the model is important for its intended use, an open software to convert the model from Modelica to a more suitable environment is needed. This will be provided by the OpenModelica editor and the tools of Bodylight.js [76] which convert the model to a web component which can be visualized in the Bodylight editor. OpenModelica is capable of exporting the model in the format of functional mock-up unit (FMU) which can be later converted to a javascript module with the Bodylight editor. For the estimation of functions based on data, the SciPy library is used, namely the curve_fit function which implements the Levemberg-Marquardt algorithm. The library is in language Python.

The versions of the software are the following:
OpenModelica editor 1.19.2 dev.beta1
Bodylight compiler 2.0.37
Bodylight editor 2.0.40
Python 3.8.12
SciPy library 1.10.0

Chapter 3

Implementation

3.1 Overview of the model

The model builds upon Sorensen's model - it uses the same mathematics for metabolite circulation across organs and uses his equations as foundations for determining other more detailed parameters. The model contains organ models for the brain, heart, liver, kidneys, gut, adipose tissue, and skeletal muscle. The lungs and red blood cells are included as metabolic sinks and sources but are not modeled as organs. Sorensen didn't model intracellular processes, only vessel and interstitial ones. The separation between intra- and extracellular space and metabolite exchange is modeled similarly to his separation of interstitial and vascular space. To avoid a double membrane modeling, where possible, vascular and interstitial space is combined into one extracellular space, except for muscle.

3.1.1 Implicitly modeled tissues

As can be seen from summing the masses of explicitly modeled tissues, it is clear that a part of the total body mass is unaccounted for. This should mainly be bones and skin. It is not clear what exactly does the energy metabolism of bones look like, but it seems that it primarily utilizes glycolysis since there is little oxygen in the environment.[64] The skin uses glucose as a primary source of energy with the majority of glucose being converted to lactate.[65] It is assumed that these tissues should be implicitly captured in the measurements conducted on the muscle or adipose tissue. In the model, the bones are combined with skeletal muscle as part of the muscle tissue module based on their physical proximity. The skin is neighboring the subcutaneous fat tissue (which is the major fat tissue), and so it is modeled that the skin is a part of the adipose tissue compartment.

3.1.2 Metabolite circulation

Each organ follows a structure for metabolite exchange. Adapting the work of Carstensen et al.[14], Sorensen's function's have been vectorized. First, all metabolites inflowing into the organ from other organs are mixed to produce

an input mass flow. In the current setting, the circulating metabolites are glucose, lactate, amino acids (represented by a single metabolite), glycerol, and insulin. Glucagon is modeled in a more simple system and is not modeled as circulating.

$$m_i^{in} = \mathbf{Q}_i^{in} \cdot \mathbf{C}_i^{in} \tag{3.1}$$

Where m_i^{in} is the mass of the i-th metabolite inflowing the organ (unit/min), $\mathbf{Q}_i^{in}$ is a vector of blood flow rates from input organs in dl/min, $\mathbf{C}_i^{in}$ is a vector of concentrations (unit/dl) from input organs. Selected metabolites in the extracellular space can move across cell membrane, based on gradients. The exchangeable metabolites are glucose, lactate, amino acids and glycerol.

$$m_i^{cell} = k_i(C_i^{out} - C_i^{cell}) \tag{3.2}$$

Where m_i^{cell} is the mass flow of the i-th metabolite to the cell, k_i is the i-th membrane transport constant (dl/min), C_i is the concentration of the i-th exchangeable metabolite in the extracellular space (out) or the intracellular space (cell). The metabolites also actively leave the extracellular space.

$$m_i^{out} = Q_i^{out} C_i^{out} \tag{3.3}$$

$$Q_i^{out} = \sum Q_i^{in} \tag{3.4}$$

Where m_i^{out} is the mass flow of the i-th metabolite out from the organ, Q_i^{out} is a scalar output blood flow rate in dl/min, C_i^{out} is a scalar extracellular concentration at the given organ. The sum of input flows is the output flow.

The sum of these three mass flows m_i^{out}, m_i^{in}, m_i^{cell} determines the rate of accumulation of a metabolite in the extracellular space. In a stable state, they should sum to zero. Blood flows are assumed constant, like in Sorensen's model. The tissues are connected as shown in figure 3.1.

3.1.3 Intracellular reactions

The scheme of Carstensen et al. is adapted and the following intracellular metabolites are modeled: glucose, glucose-6-phosphate (G6P), glyceraldehyde-3-phosphate (G3P), pyruvate, lactate, acetyl coenzyme A, glycogen, amino acids, glycerol. The system of modeled reactions is depicted in the figure 3.2.

Almost all of the function shapes were taken from the work of Pratt et al. [71]. Most often the reactions are modeled as dependent on normalized concentrations of metabolites which makes setting up basal rates more clear. The normalization is by basal mass. The metabolites are modeled as a pool from which reactions give and take. There two pools in the cell - exchangeable metabolites (transfer pool) and molecules that do not leave the cell (locked pool).

After entering the cell, glucose is phosphorylated to G6P. This is modeled as Michealis-Menten reaction with product inhibition. The liver has one extra equation to model this reaction, which is described in the section of liver.

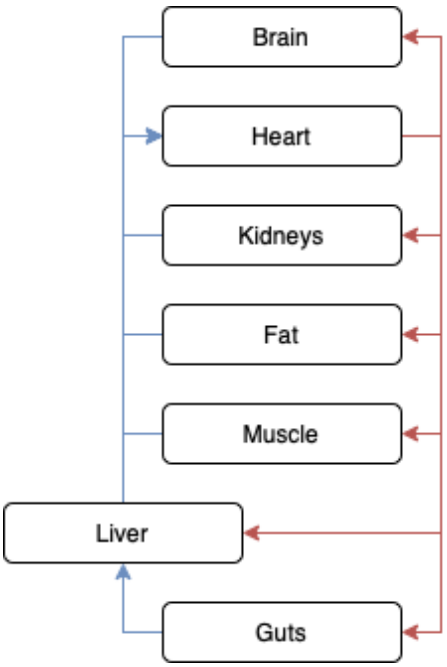

Figure 3.1: Blood flow circulation between modeled organs

$$r = v_{max} \frac{C_{glu}}{(K_m + C_{glu})} \frac{1}{(1 + \frac{C_{g6p}}{K_i})} \tag{3.5}$$

Where r is the reaction rate (in mg/min), v_{max} is the maximum velocity, K_m is the half-saturation constant, C is the concentration of a metabolite and K_i is the inhibitory constant. The units dependent on whether we use normalization or not, and they will be specified depending on the context. The reverse reaction is modeled by a Michealis-Menten equation without inhibition, because glucose is only a minor inhibitor. [90]

$$r = v_{max} \frac{C_{g6p}}{(K_m + C_{g6p})} \tag{3.6}$$

G6P can be converted into G3P, G3P to pyruvate, and pyruvate to lactate or ACoA. Amino acids are assumed to be converted directly to pyruvate, and also lactate can be turned to pyruvate. Glycerol is converted to G3P. All of these reactions are modeled in the following way

$$r = kC \tag{3.7}$$

where k is the basal rate in mg/min and C is the normalized metabolite mass driving the reaction.

Glycogen synthesis is modeled as $r = kC$ with tanh inhibition representing reaction inhibition by filling the glycogen stores.

$$r = k_1 C_{in}(1 + \tanh(k_2(k_3 - C_{outmax}))) \tag{3.8}$$

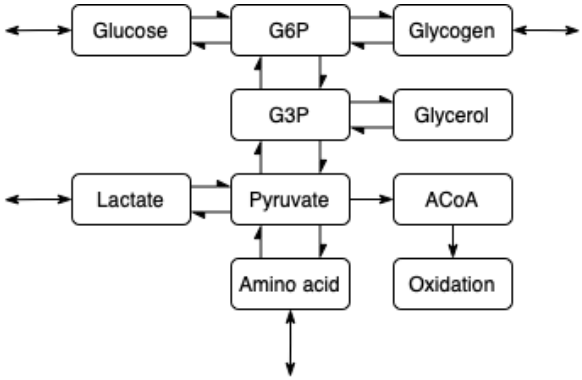

Figure 3.2: All possible intracellular reactions in the model

Glycogenolysis is modeled as a tanh function which decreases significantly as glycogen stores get depleted.

$$r = k_1 \tanh(k_2 C_{in}) \tag{3.9}$$

The effects of insulin, glucagon or glucose are modeled as multiplicative and are always assumed to equal one in the basal state. As discussed in the Theory section, this approach is inspired by Sorensen's work.

$$r_{reg} = E(X)r \tag{3.10}$$

Where r_{reg} is the regulated rate, $E(X)$ is the effect function depending on the normalized concentration of a certain regulator (insulin, glucagon or glucose). There is one exception to this, and that is the ACoA oxidation. In theory this process should be limited, and therefore the $E(X)$ effect is put inside the tanh argument.

3.1.4 Volumes and Flows

Sorensen provides his estimates of blood flows and volumes for individual organ compartments on page 36 of his thesis. [80] The peripheral compartment volume and blood flow are calculated as the difference of the total volume/blood flow minus the rest of the organs. The peripheral compartment combines the volumes of skeletal muscle and adipose tissue. The interstitial and intracellular volumes of the heart&lungs tissue are also added to the periphery compartment. However, the heart&lungs block has its own blood flow and vessel volume. It is important to note, that the peripheral compartment volume also includes other residual tissues, for example, bones and skin. Since one of the goals of this model is to model the skeletal muscle and adipose tissue separately, this has to be solved. All of the volumes and flows are in litres and in litres/min.

The peripheral compartment has 1.26 litres in equilibration volume (combined veins with capillaries), 6.74 litres in interstitial (IS) volume and 19.65 litres in intracellular (IC) volume. From rat heart studies [7], heart extracellular (EC)

and intracellular (IC) volumes can be estimated. If we assume the heart mass to be 310 g [96] and use dry to wet mass ratio of 0.2, then the EC volume is circa 0.049 litres, and the IC volume is 0.159 litres.

The intracellular volume of Sorensen's periphery module is circa 0.7 of the total volume of the compartment. Muscle consists circa 75% of water.[31] Assuming the same 0.7 ratio for skeletal muscle, for 27 kg of muscles that would be 6.07 litres in EC and 14.18 litres in IC space (the muscle mass is estimated in the Skeletal muscle section). The adipose tissue water content is estimated at 15% [67]. Using 10 kg of adipose tissue mass (as Sorensen) and the same ratio, that would be 0.45 litres in EC and 1.05 litres in IC space. The lung water content is circa 80% [59]. The lung mass is 840 grams [63], and with the same ratio as above that would produce 0.20 litres in EC and 0.47 litres in IC space.

The heart and lungs interstitial volumes are included in the periphery. Subtracting heart and lungs EC volumes from the peripheral interstitium volume (6.74 litres) should correct for that with little error, and give 6.42 litres. The equilibration to extracellular volume ratio for the peripheral compartment is circa 0.16. Applying this ratio to skeletal muscle and adipose tissue gives 5.10 litres of muscle interstitium and 0.38 litres of adipose interstitium. The remainders are equilibration volumes, that is 0.97 litres for skeletal muscle and 0.07 litres for adipose tissue.

Summing up the above calculated intracellular spaces, that gives 15.75 litres, which is 3.9 litres short of the peripheral intracellular volume (19.65 litres). Interstitial volumes give 5.69 litres, which is 1.05 litres below the peripheral interstitium (6.74 litres). Summing skeletal muscle and adipose tissue equilibration volumes gives 1.04 litres which is 0.22 litres lower than the peripheral volume (1.26 litres). The reason for not including the heart&lungs in the equilibration volume sum is that Sorensen assigned the heart&lungs equilibration volume to the heart&lungs block.

One tissue that is not accounted for is the bone, which contains circa 30% of water. [59] 15% of the human body mass is the bones, which for a 70 kg man is 10.5 kg, with water content of 3.15 litres. This can explain 60% of the missing volume. Another tissue that fills the remaining gap is the skin, with 64% water content [59] and a mass of 3.5 kg [52]. That gives 2.24 litres water content. Because of their physical proximity, the bone compartment volume is added to the muscle tissue volume. The skin is added to the adipose tissue.

Using the same ratios as above, the total water mass for bones and skin was added to the muscle and adipose tissue, respectively. The lungs are modeled only as a sink and source and not a full organ, so their volume is added to the Heart compartment. The interstitial and intracellular volumes in litres are summarized in the table 3.1.

Sorensen's peripheral blood flow was taken as the remainder of blood flow to match cardiac output, making it 1.80 l/min. From [21] it is estimated that skeletal muscle blood flow is circa 0.92 l/min and adipose tissue blood flow is

Tissue	Interstitium	Intracellular
Brain	0.45	0.86
Heart and Lungs	0.21	0.63
Liver	0.6	1.15
Gut	0.52	1.01
Kidney	0.09	0.18
Hepatic artery	-	-
Muscles	5.89	16.39
Adipose	0.94	2.62

Table 3.1: Interstitial and intracellular volumes of the compartments

circa 0.23 l/min. That means circa 0.65 l/min is unallocated. The skin has blood flow circa 0.07 l/min (2 ml/100 g/min [41], 3.5 kg mass). The bones have blood flow circa 0.19 l/min (1.8 ml/100 g/min [35], 10.5 kg mass). As discussed above, the bones are grouped with muscle, and skin is grouped with adipose tissue. It is uncertain which other tissues does the still unallocated blood flow perfuse. The ratio between adipose compartment blood flow and muscle compartment blood flow (with bones and skin added) is circa 0.27. The remaining blood flow is added to the modules to maintain this ratio.

The equilibration volumes and blood flows have to be corrected for red blood cell (RBC) volume and if a metabolite can enter them. Sorensen calculated that if a metabolite can enter RBCs, it can use 84% of the total equilibration volume or blood flow; if not, 60% is available. Glucose can enter RBCs [80], and it seems that also lactate [29], glycerol [13] and amino acids [84] can. Insulin can't enter a RBC. [80]

Tissue	Equilibration volume full	RBC perm.	RBC imperm.
Brain	0.41	0.35	0.25
Heart and Lungs	1.64	1.38	0.98
Liver	0.9	0.76	0.54
Gut	0.71	0.60	0.43
Kidney	0.68	0.57	0.41
Hepatic artery	-	-	-
Periphery	1.26	1.04	0.75
Muscles	1.12	0.94	0.67
Adipose	0.18	0.15	0.11

Table 3.2: Full, RBC permeable and RBC non-permeable equilibration volumes

Tissue	Blood flow Full	RBC perm.	RBC imperm.
Brain	0.7	0.59	0.42
Heart and Lungs	5.2	4.37	3.12
Liver	1.5	1.26	0.9
Gut	1.2	1.01	0.72
Kidney	1.2	1.01	0.72
Hepatic artery	0.3	0.25	0.18
Periphery	1.8	1.51	1.08
Muscles	1.4	1.19	0.85
Adipose	0.4	0.32	0.23

Table 3.3: Full, RBC permeable and RBC non-permeable blood flows

3.1.5 Basal concentrations and constants

All metabolites are expressed in glucose equivalents. As Sorensen derived, plasma concentration is 92.5% of whole-blood concentration and blood concentration is 84% of whole-blood concentration ([80], p. 45), which was used to convert the values found in the literature. For arterial whole-blood concentration (heart compartment): glucose - 97.3 mg/dl ([80], p. 126), lactate 10.7 mg/dl [11], glycerol 0.7 mg/dl [88]. For amino acids, an average of glutamine and alanine concentrations [57] was taken, 4.6 mg/dl. The arterial plasma concentration of insulin is set to 1.5 mU/dl.

It was difficult to find information regarding the intracellular concentration of metabolites. One helpful piece of information is gradient transport. Most of the time information was available on whether an uptake was positive or negative for a metabolite. Since all transport in the model is modeled as simply by the gradient (enhanced by insulin in the case of glucose), it can at least be said if the concentration is lower or higher than in the extracellular space. The negative impact of possibly imprecise intracellular concentrations is reduced by normalizing all metabolites in the cell by their basal masses. Still, if a basal mass is assumed too low, the reaction dynamics will be too fast; and if too high, the reaction dynamics will be too slow. The reason for this is that a small amount of metabolite will double more quickly and hence swiftly stimulate all the related reactions. In the model, the basal concentrations of glucose, lactate, amino acids, and glycerol are usually within the range of 0.1-10 of their extracellular concentrations which seems physiologically sensible. Another helpful source was the model by Pratt et al. [71] from which intracellular liver and muscle concentrations for glucose and G6P were taken - liver: 8 mmol/l glucose; muscle: 0.5 mmol/l glucose, 0.13 mmol/l G6P. The pyruvate concentration is set to 0.13 mmol/l [30]. The concentrations of G3P and ACoA are set to the same level as pyruvate. The glycogen basal concentration in the liver is estimated to match 50% of the maximum 100 grams. For the muscle, maximum of 400 grams was set, again in basal state at 50% maximum.

From knowing the whole-blood concentrations, intracellular concentrations, blood flows, and basal metabolite flows, the transport constants k can be calculated. Assuming a steady state, then the net outflow from the tissue has to equal the net outflow from the cellular membrane. The basal flows are determined for each tissue separately in the section below. It should be noted that often only the net inflows for a certain metabolite are known and in case of reversible reactions (often lactate-pyruvate shuffling) the base reactions had to be chosen arbitrarily.

3.1.6 Curve fitting

To fit a tanh curve, at least four data points are needed in theory. The tanh curves are used to model the effects of insulin and glucagon on metabolite flows. These flows are rarely known directly and most of the time are calculated based on uptake-release organ functions describing how insulin or glucagon affects organ uptake or release of a metabolite. These calculations are based on the assumption of a steady state in which metabolite concentrations are stable and flows sum to zero. This is possible because all of the insulin or glucagon effects are isolated and assume a euglycemic clamp. For calculations, 4-6 insulin or glucagon levels are taken, ranging from hypo- to hyper- states. These levels are inputted to the uptake-release organ function from which the steady state for all intracellular metabolites is calculated. Having 4-6 data points for each flow, the selected flows can be fitted with tanh curves.

3.2 Tissue models

3.2.1 Brain

The brain is one of the most metabolically active organs which utilizes glucose as its main energy source. Sorensen, based on studies of brain glucose uptake, modeled it to be 70 mg/min ([80], 53). 8% of the uptaken glucose gets converted to lactic and pyruvic acid ([80], 51). Van Hall in an review states that the brain netly releases 5 mg/min of lactate [89]. Sorensen further assumes that brain glucose uptake is constant under normal physiological conditions, since 'glucose and oxygen uptake remained essentially unchanged' in experiments on dogs in the range of 25-245 mg/dl. In humans, 'when circulating glucose levels fall below ... 40 to 50 mg/dl ... [brain] glucose uptake begins to decrease'. ([80], 52)

Basal flow rates

The glucose influx during normal glucose levels is sufficient to saturate the hexokinase reaction. [20]. Hexokinase is saturated while intracellular glucose is greater than 0.8–1.0 mmol/l. [56] The plasma-brain ratio is circa 0.2 [20] meaning that interstitial glucose is circa 1 mmol/l at 5 mmol/l of blood glucose levels. Intracellular glucose should then be similar to the interstitial levels at a basal state. The Michealis-Menten parameter K_m for hexokinase in the brain is circa 0.05 mmol/l [20]. Resting brain hexokinase activity in brain

is 5% of its maximum capacity due to its inhibition by glucose-6-phosphate (G6P). [56] The brain is essentially insensitive to insulin and Sorensen models it to be free of insulin and glucagon regulation. ([80], 52)

The brain is modeled to pick up 70 mg/min of glucose, oxidizes 65 mg/min to CO_2 and converts 5 mg/min to lactate ([80], 51) which outflows into blood. Assuming full saturation of the hexokinase

$$70 = v_{max} \cdot 0.05 \tag{3.11}$$

and solving the equation for v_{max} gives $v_{max} = 1400$ mg/min. If we normalize G6P concentration by its basal concentration, then at a steady state normalized G6P is equal to one, leaving

$$0.05 = \frac{1}{1 + \frac{1}{K_i}} \tag{3.12}$$

From here K_i, in normalized units, is 0.056. G6P to G3P and G3P to pyruvate have basal rates of 70 mg/min. The pyruvate to lactate reaction is set to a basal rate of 10 mg/min and a counter-reaction of lactate to pyruvate has reaction rate 5 mg/min. Conversion of pyruvate to acetyl-CoA (ACoA) has basal rate of 65 mg/min. Oxidation of ACoA is modeled as being at max 105% of the basal rate (100%), oxidating 65 mg/min of glucose at the basal ACoA concentration and following the function $65 \cdot 1.05(\tanh(1.85C^N))$, where C^N is normalized ACoA concentration.

3.2.2 Heart and arteries

The heart utilizes glucose as a minor energy substrate – most of its energy is provided by the oxidation of fatty acids. There is also net lactate uptake, which is driven towards oxidation. 70% of cardiac energy metabolism is provided by fatty acids [55] and 90% is provided by fatty acids and carbohydrate metabolism [1]. 50% of the pyruvate oxidized comes from lactate [82]. The heart has a metabolic rate of 0.093 kcal/min [96]. If we assume 4 kcal/g of glucose oxidation, that is circa 2.3 mg/min of lactate uptake and glucose uptake at a basal state, modeled both as 3 mg/min. Lactate oxidation depends on arterial lactate concentrations and can vary [82]. The hexokinase parameters and glucose and G6P concentrations are assumed to be the same as in the muscle.

The effect of insulin

The heart tissue is sensitive to insulin, and glucose can become a major substrate (60-70% of energy demands) after a carbohydrate rich meal [38]. If we assume 70% energy is covered by glucose after a carbohydrate rich meal, that is circa 16 mg/min, a circa 5.3-fold rise in uptake would be required. After such meal, plasma glucose rises circa 1.4-fold and insulin grows circa 8-fold at peak compared to basal levels [58]. Dividing by the effect of glucose (which is non-linearly limited by hexokinase) would leave the insulin multiplier to be circa 4. The function for the effect of insulin on cardiac metabolism

is assumed to have the same sigmoid shaped curve as in the muscle, scaled down to multiply uptake at most 4 times.

$$E_{uptake}(I^N) = 2.5 + 1.62 \tanh(0.39(I^N - 5.2)) \tag{3.13}$$

It is assumed that all extra glucose taken up is used for oxidation and that insulin targets GLUT4 translocation and the same glycolytic reactions in the heart as in the skeletal muscle – hexokinase and G6P to G3P conversion. To estimate the effect on membrane transport we have to first calculate the predicted uptake r from

$$r = E_{uptake} r_B \tag{3.14}$$

where r_B is the basal uptake rate. To find the insulin effect on membrane glucose transport, the outflow glucose concentration C_{out} must be found.

$$C_{out} = C_{in} - \frac{r}{Q} \tag{3.15}$$

where Q is the input blood flow. From the calculations (not shown) it could be seen that due to large blood flow and relatively small glucose uptake, the interstitial glucose stays almost constant (decrease by 0.2 mg/dl at 8-fold insulin increase). The effect of insulin on membrane transport E_{glut4} is therefore modeled as equalling E_{uptake}. The glucose to G6P and G6P to G3P reactions are also stimulated with the same E_{uptake} function. Furthermore, it is assumed that insulin increases glucose oxidation indirectly through decreasing fatty acid oxidation (as shown for muscle in [21]). This effect is modeled as a direct influence of insulin on pyruvate to ACoA conversion and ACoA oxidation, taking into account lactate oxidation which is assumed constant.

$$E_{oxid}(I^N) = 1.81 + 0.87 \tanh(0.39(I^N - 5.2)) \tag{3.16}$$

The oxidation function has the same slope and shift parameters as the muscle glucose uptake function. The oxidation of pyruvate is modeled as linearly increasing up until saturation at 85% of basal energy needs, that is circa 20 mg/min in glucose equivalents.

$$r_{ACoA} = r^B_{ACoA} 3.33 \tanh(0.31 C^N_{ACoA}) \tag{3.17}$$

3.2.3 Liver

The liver can handle glucose in multiple ways. It has modest glycogen stores (circa 100 g) and also produces glucose through gluconeogenesis. Sorensen models the basal hepatic glucose production at 155 mg/min ([80], p. 75). With respect to that, 68% can be estimated to be provided by glycogen ([80], p. 80), hence circa 105 mg/min. The net splanchic glucose release was measured to be 115 mg/min. Based on dog studies, Sorensen ascribed 20 mg/min of the uptake to the liver and 20 mg/min to the other splanchic

tissues. ([80], p. 76) The uptaken glucose can be stored, oxidated or converted to fatty acids (de novo lipogenesis). It is assumed that at basal state, the uptaken glucose is utilized and not stored. Conversion to fatty acids should also be relatively small in the basal state. [6] Because of that, the 20 mg/min uptake is modeled as being entirely oxidated.

After glucose enters the cells it can be phosphorylated not only by the hexokinase enzyme but also by the glucokinase enzyme which has both higher maximal rate and affinity, and isn't inhibited by glucose-6-phosphate. Whereas hexokinase follows Michealis-Menten kinetics, glucokinase follows the Hill equation [42]

$$r = v_{max} \frac{1}{1 + (\frac{K_m}{C})^n} \tag{3.18}$$

where v_{max} is the maximum velocity K_m the mid-point, C is the concentration of the metabolite and n is the Hill coefficient.

From in vitro data, Stanley et al. estimated glucokinase maximum velocity to be 1.01 μmol/min per gram of liver tissue [81]. In a textbook, Baynes & Domynczak use the number 1.5 μmol/min per gram of liver tissue [8]. An average is taken – 1.25 μmol/min per gram of liver tissue, or 338 mg/min, assuming 1500 g liver mass ([80], p. 235). Hexokinase maximum velocity is circa 0.1 μmol/min per gram of liver tissue, or 27 mg/min [8] and K_m is less or equal to 0.1 mmol/l [12], assumed to be 0.1 mmol/l. The inhibition constant of hexokinase by G6P is assumed to be the same as in the brain 0.2 mmol/l. [86] The glucokinase mid-point saturation is 8 mmol/l and Hill coefficient 1.78. [42]

Glycogen synthase is stimulated by glucose-6-phosphate. From in vitro data it seems that such stimulation is linear up to a saturation threshold [93]. Since the reaction rate of glycogen synthesis is modeled as a product of G6P concentration and the basal rate, determining glycogen synthesis basal rate is important for modeling liver glucose uptake. G6P levels could rise in the event of increased glucose uptake. Sorensen provides a function for the effect of liver plasma glucose on glucose uptake, however, there are big differences in oral glucose test and intravenous glucose test results. The difference is probably caused by the lack of modeling of the effect of incretins [69] which are not included in the Sorensen's model, nor in the current model. Furthermore, in a review Hatting et al. say 'hyperglycemia alone suppresses hepatic glycogenolysis with only minimal effects on glycogen storage. Only the combination of hyperglycemia and hyperinsulinemia has a significant effect on hepatic glycogen synthesis'. ([33], p. 23) It could therefore potentially be misleading to separate the action of insulin and elevated glucose levels on glycogen synthase.

Based on Sorensen's liver glucose uptake and production glucose functions, net glucose production can be calculated under insulin and glucagon stimulation. A high basal rate for glycogen cycling will require only small nominal multiplications to achieve the calculated increased (or decreased production).

This would generally make the glycogen reactions relatively insensitive to insulin or glucagon. In the context of Hatting et al. it seems more plausible to assume the other scenario - a low basal glycogen synthesis rate which would necessitate a high multiplicative effect of insulin, which is in line with 'only hyperglycemia and hyperinsulinemia has a significant effect on hepatic glycogen synthesis'. ([33], p. 23) For these reasons, the model assumes a basal glycogen synthesis rate of 5 mg/min.

As calculated above, net glycogenolysis is 105 mg/min, hence basal glycogenolysis is $5 + 105 = 110$ mg/min. Conversion of G6P to G3P and G3P to PYR has the basal rates of 20 mg/min. PYR to ACoA has also basal rate of 20 mg/min, and ACoA oxidation as well.

Basal gluconeogenesis

Liver gluconeogenesis mainly uses lactate, amino acids and glycerol. Pyruvate is also a substrate but forms only 4% of gluconeogenesis ([80], p. 81) and its mass flow is divided between the three named substrates. After such correction, the percentages for the substrates are; lactate 56%, amino acids 30%, glycerol 14%. The basal flow of lactate to pyruvate is 38 mg/min, pyruvate to lactate 10 mg/min, amino acids to pyruvate 15 mg/min and glycerol to G3P 7 mg/min. Pyruvate to G3P basal rate is 43 mg/min, G3P to G6P is 50 mg/min. The reaction of glucose-6-phosphate to glucose follow Michealis-Menten kinetics with K_m = 2-3 mmol/l, and van Schaftingen states that G6P levels are in the range of 0.05-1 mmol/l. [90] It is assumed that basal G6P concentration is 0.45 mmol/l and $K_m = 2.5$ mmol/l. The sum of GLU to G6P reactions and G6P to GLU has to produce net liver glucose outflow of 135 mg/min in the basal state. Assuming liver glucose concentration of 8 mmol/l, the maximum velocity of the G6P to GLU reaction is circa 409.5 mg/min.

$$135 = v_{max}\frac{0.45}{(2 + 0.45)} - r_{gk} - r_{hk} \tag{3.19}$$

where v_{max} is the maximum velocity of G6P to glucose conversion, and gk and hk are glucokinase and hexokinase.

The effect of insulin

Insulin stimulates glucokinase, glycogen synthesis, glycolysis, lipid synthesis and inhibits gluconeogenesis, glycogenolysis and fatty acid oxidation. [22] [2] [32] Sorensen assumed, based on dog studies, that insulin can increase the basal uptake up to two times after a delay. ([80], p. 117). Glycogen stores are filled first and in case of excessive carbohydrates will be transformed to fatty acids. Furthermore, insulin stimulates glycolysis as the part of committing glucose-6-phosphate to glycolysis. [32] Since insulin inhibits fatty acid oxidation, carbohydrates have to cover for the difference. The liver has metabolic basal rate of 0.21 kcal/min [96], with 4 kcal/g of glucose oxidation that is at maximum circa 50 mg/min of glucose oxidation. In the muscle tissue, glucose oxidation almost replaced fatty acids at circa 7-fold insulin increase. [45] Because of that, it is assumed that at that level, 70% of the

energy requirements is provided by glucose. De novo lipogenesis is thought to be less than 5% of triglycerides released in the liver in the fasted state which increases by 25% in the fed state. [70] For the basal state, very-low-density lipoprotein synthesis is thought to be circa 10 mg/min (in fatty acid equivalents) [34]. Palmitic acid has 16 carbons, which would require 2.67 glucose molecules to synthesize it. 5% of 10 mg/min is 0.5 mg/min, which in glucose equivalents is circa 1.33 mg/min. It is therefore assumed that it shouldn't be a significant route for glucose disposal, at least in a healthy liver. For the model, it is assumed that all of the additional uptaken glucose above oxidation is directed towards glycogen synthesis.

Sorensen also estimated a function for the effect of insulin on hepatic glucose production ([80], p. 86). Gastaldelli et al. measured that glycogenolysis is completely suppressed and gluconeogenesis reduced by 20% in euglycemic insulin stimulation (circa 74 mU/min infusion) [28]. Since Sorensen's function already suppresses hepatic glucose production to circa 20 mg/min from 155 mg/min at 2 normalized liver insulin levels, it is assumed that glycogenolysis is almost fully suppressed at that level and the rest is attributable to gluconeogenesis. Insulin regulates gluconeogenesis through inhibiting pyruvate kinase [32], which is represented in the model as inhibiting the reaction PYR to G3P. Insulin also inhibits the G6P to glucose reaction [90] and stimulates glucokinase [2]. It is assumed that the last two named reactions are affected equally by insulin to produce the calculated net production.

First, the reactions related to pyruvate and G3P are solved. The conversion of pyruvate to ACoA is modeled as being directly influenced by insulin, even though the relation is likely indirect through fatty acid modulation, like in the muscle as described in [21]. Based on the assumptions on oxidation above, a function of insulin's effect on glucose oxidation is proposed:

$$E^I_{oxid}(I) = 0.938 + 0.938 \tanh(0.23(I^N - 0.7)) \tag{3.20}$$

The inflow of gluconeogenic substrates has to be considered, since both lactate and amino acid concentrations change as discussed in the section on kidneys. Arterial lactate rises, amino acids stay the same, or decrease. From calculations (not shown) it seems that at assumed basal rates, the total lactate and amino acid inflow into the liver slightly rises under insulin stimulation. It is assumed that at 5-fold insulin increase, the sum of lactate and amino acid inflow rises 1.15 times. This effect is modeled as circa linearly increasing with insulin. Assuming constant G3P and pyruvate levels, the pyruvate to G3P rate can be calculated.

$$r_{lac} + r_{aac} + 20 = r_{oxid} + r_{pyr-g3p} \tag{3.21}$$

Where $r_{pyr-g3p}$ is the insulin-regulated reaction of PYR to G3P and the rest are reaction rates of pyruvate formation, the constant 20 represents the G3P to PYR flow. From that the insulin effect on PYR to G3P can be found

$$E_{pyr-g3p}(I^N) = 0.94 - 0.1 \tanh(0.57(I^N - 2.18)) \tag{3.22}$$

Reduced glycerol inflow is modeled as corresponding to the relative decrease in its production in the adipose tissue; using the same insulin effect function

$$E_{lipo}(I^N) = 1.13 - 0.63 \tanh(0.71(I^N - 0.71)) \tag{3.23}$$

The G3P levels would fall due to reduced G3P inflow from gluconeogensis and glycerol, but this is modeled as compensated by enhanced G6P to G3P conversion, which is in line with insulin stimulating glycolysis. [32] G6P levels are also assumed to be in the basal state.

$$E_{g6p-g3p}(I^N) = 1.08 + 0.45 \tanh(0.49(I^N - 1.35)) \tag{3.24}$$

With this, the glycolytic and gluconeogenic path from G6P on is solved.

Second, glycogen synthesis and breakdown together with glucose conversion to G6P is discussed. Sorensen's functions describing the insulin effect on liver release ($E^I_{HGP}(I)$)and uptake ($E^I_{HGU}(I^N)$) are multiplied by the basal rates to obtain net outflow of glucose r.

$$r = 20E^I_{HGU}(I^N) - 155E^I_{HGP}(I) \tag{3.25}$$

After finding net glucose inflows as predicted by Sorensen, liver glucose extracellular concentration C_{out} can be found, since C_{in} is assumed constant under euglycemia.

$$C_{out} = C_{out} - \frac{r}{Q} \tag{3.26}$$

Where Q is the liver output blood flow for glucose. For a stable state, the flow r has to equal membrane transfer to the cell.

$$C_{cell} = C_{out} - \frac{r}{k} \tag{3.27}$$

Where C_{cell} is the glucose concentration in the cells, k is the glucose membrane transport constant. Once we know the intracellular glucose concentration we can calculate the net glucose to G6P flow without insulin stimulation by summing the hexokinase, glucokinase and G6P to glucose rates. The difference between this flow and the target r net flow is corrected by insulin modification function on glucokinase and G6P to glucose. It is assumed that the effect is split equally between these two reactions.

$$E_{gk}(I^N) = 1.28 + 0.96 \tanh(1.34(I^N - 1.22)) \tag{3.28}$$

$$E_{G6Pase}(I^N) = 1.28 + 0.96 \tanh(1.34(I^N - 1.22)) \tag{3.29}$$

Where E_{gk} is the effect on glucokinase.

Glycogenolysis is completely inhibited during insulin stimulation, which is in line with Sorensen's function on hepatic glucose production which drops sharply even at two-fold insulin increase. It is therefore assumed that any hepatic glucose production during hyperinsulemnia comes from

gluconeogenesis. It then follows that the net uptake of glucose plus net gluconeogenesis has to flow into glycogen stores to maintain stable G6P levels. During hypoglycemia, glycogen breakdown is stimulated and synthesis reduced to maximize glucose output from the liver. It is therefore assumed that under normal or low insulin levels, all gluconeogenesis flows out of the liver and none to storage. The glycogenolysis during this range of insulin levels can be calculated as hepatic glucose release (from Sorensen) minus net gluconeogenesis minus hepatic glucose uptake (from Sorensen). To these rates of glycogen synthesis and breakdown, the baseline of 5 mg/min was added and the rates were normalized. The resulting normalized rates for glycogen synthesis were fitted

$$E_{synth}(I^N) = 5.41 + 5.4 \tanh(1.79(I^N - 1.64)) \tag{3.30}$$

Glycogenolysis is suppressed not only by insulin, but also by glucose. To estimate the effect of insulin on glycogenolysis, we have to take into account that during insulin stimulation, liver glucose is lowered and it does not inhibit liver glycogenolysis as much. To estimate this effect, Sorensen's function for the inhibition of hepatic glucose production $M^G_{HGP}(G^N_L)$ is used with the calculated C^N_{out} $(= (G^N_L))$.

$$M^G_{HGP}(G^N_L) = 1.42 - 1.41 \tanh(0.62(G^N_L - 0.497)) \tag{3.31}$$

The normalized rate of glycogenolysis is divided by the calculated effect of glucose to correct for the glucose effect and an insulin multiplier function for glycogenolysis is estimated.

$$E_{break} = 1.8 - 1.8 \tanh(1.75(I^N - 0.73)) \tag{3.32}$$

The glucagon effect

Glucagon also affects liver pathways; stimulating glycogenolysis[80], inhibiting glycolysis[37], inhibiting glucokinase[17], stimulating G6Pase[32] and stimulating liver protein usage[72]. Sorensen modeled liver glucagon as affecting hepatic glucose production and provided a function for the effect. The production rises sharply and then the effect gradually drops to 0.5 of its above-basal value. In other words, if the glucagon initially rises glucose production to $r_{HGP} = 2r^B_{HGP}$, eventually, it will become $r_{HGP} = 1.5r^B_{HGP}$. Sorensen's function describing the initial maximum effect is:

$$E^{max}_{HGP}(\Gamma^N) = 2.7 \tanh(0.39\Gamma^N) \tag{3.33}$$

Glucagon's effect on glycolysis is quick with decreasing amplitude while net gluconeogenesis gets affected only gradually. [72] It is assumed that at time near zero of the glucagon step, the entire effect in increased glucose production is attributable to glycogenolysis, while at stable point circa 16% of the increased effect are provided by gluconeogenesis raising (estimated from [72]). The glucagon effects can therefore be calculated in two scenarios - near the step increase in glucagon and after stabilization.

After the glucagon step, hepatic glucose release sharply rises. To obtain such outflow of glucose at blood euglycemia, extracellular levels have to change:

$$C_{out} = C_{in} + \frac{r}{Q} \tag{3.34}$$

where r is the predicted net glucose outflow (from $r = E_{HGP}^{max} - r_{HGU}$) and Q is liver blood flow for glucose. From there intracellular glucose C_{cell} concentration is

$$C_{cell} = C_{out} + \frac{r}{k} \tag{3.35}$$

where k is the membrane transport constant for glucose. The increased glucose levels affect glucokinase. Hexokinase is thought to be constant due to it's relatively small role. The G6P to GLU flow can be calculated from the net outflow plus the glucokinase and hexokinase flows. It is modeled that G6P concentration remains at basal levels since G6Pase is stimulated by glucagon [32] and glucokinase activity is reduced [17]. The effect of glucagon is modeled as being split half-half between G6Pase and glucokinase to achieve the target net outflow of glucose r.

$$E_{gk}^{max}(\Gamma^N) = 1.07 - 0.63\tanh(0.42(\Gamma^N - 0.74)) \tag{3.36}$$

$$E_{G6Pase}^{max}(\Gamma^N) = 0.55 + 0.98\tanh(0.4(\Gamma^N + 0.25)) \tag{3.37}$$

Shortly after the glucagon step, there should be no apparent changes in gluconeogenesis or glycolysis, and these are assumed to be in the basal state. Since G6P levels are also assumed to be in the basal state, glycogen synthesis is in the basal state. Glycogenolysis rate has to equal:

$$r_{break} = r - r_{synth} - r_{gng} \tag{3.38}$$

where r is the net release of glucose and r_{gng} is the inflow of G6P from net gluconeogenesis. As discussed in the section on insulin effect above, glycogenolysis is affected by glucose too. This means that to obtain an isolated glucagon effect, the normalized glycogenolysis rate has to be divided by the glucose effect. After that, the glucagon effect on glycogenolysis is estimated

$$E_{break}(\Gamma^N) = 0.5 + 3.5\tanh(0.4(\Gamma^N - 0.64)) \tag{3.39}$$

When flows stabilize, gluconeogenesis is enhanced through inhibiting pyruvate kinase [37] (G3P to PYR in the model). It is assumed that glucagon has no effect on glucose oxidation as fatty acid levels should not be suppressed, as in the case of insulin. Similarly to the deduction above, glucose concentration has to rise to provide for a certain outflow (half of the maximum effect minus basal uptake). Glucokinase and hexokinase activities can be calculated, and the glucagon multiplier of the G6Pase and glucokinase can be found. As above, an

even split of the glucagon effect is assumed between glucokinase and G6Pase. The reduction for these flows in both cases is circa to 0.5 of the maximum additional effect for all glucagon levels. 16% of the extra glucose produced compared to the basal level is provided by additional gluconeogenesis, the rest is glycogenolysis. The G6P levels are modeled to stay at basal levels during glucagon stimulation. Then the rate of additional glycogenolysis is circa 0.4 of its maximal effect.

$$0.4 = \frac{r_{inf} - r^B}{r_{max} - r^B} \tag{3.40}$$

for $r_{max} \neq r^B$; where r_{inf} is the glycogenolysis rate at stable state, r_{max} is the maximal rate near the beginning of the glucagon stimulation and r_B is the basal rate. It is important to find these stable/spike ratios as these are the parameters driving how much will the glucagon response eventually decline.

In the model, glucagon increases gluconeogenesis through inhibiting the G3P to pyruvate rate. This should raise G3P concentrations and through it increase net gluconeogenesis, since G6P to G3P should remain constant because G6P is modeled to be at basal levels. The G3P levels have to rise until they produce 16% of the late glucagon effect. Glucagon increases liver protein catabolism [72] which is modeled as enhancing the rate of amino acid conversion to pyruvate. Lactate, glycerol, and amino acid input levels are assumed (at least initially) as in the basal state. The pyruvate levels are assumed constant. With increasing net gluconeogenesis, the G3P to PYR rate has to be reduced proportionately. From this, the glucagon effect on G3P to PYR is estimated

$$E_{g3p-pyr}(\Gamma^N) = 4.6 + 4.62 \tanh(-0.42(\Gamma^N + 1.49)) \tag{3.41}$$

To compensate for the reduced inflow from G3P, amino acid conversion to pyruvate is stimulated proportionately. After counting for the reduced intracellular amino acid concentration to form the necessary gradient, a glucagon multiplier for the amino acid to pyruvate reaction was estimated:

$$E_{aac-pyr}(\Gamma^N) = 2.73 + 3.52 \tanh(0.4(\Gamma^N - 2.36)) \tag{3.42}$$

The effect of glucose inhibition Both glucose and G6P have the capacity to inhibit glycogenolysis. [3] In this model, only the inhibition effect of glucose is implemented. A function was fitted to mimic the Sorensen's glucose inhibition function with the dependence on intracellular glucose levels. For intracellular glucose that would be larger than twice times the basal, the function probably underestimates, but within the typical range (which is quite narrow) of intracellular glucose levels it should work correctly.

$$E_{break}(C^N_{cell}) = 1.01 - 0.18 \tanh(1.46(C^N_{cell} - 0.94)) \tag{3.43}$$

where C^N_{cell} is normalized intracellular concentration.

3.2.4 Kidneys

The kidneys are modeled in the Sorensen's thesis only as a site of insulin clearance and glucose excretion in case of high glucose levels. Nevertheless, the kidney is capable of both gluconeogenesis, variable glucose uptake and is sensitive to insulin. [51] [58] The kidneys have varying activities across the proximal and distal tubules. In the distal tubules glycolysis is the primary source of energy and results in the production of lactate, whereas the cortex relies on fatty acid oxidation and has gluconeogenic enzymes. [51] Kidneys are capable of GLUT4 translocation in the podocytes of the glomerulus when stimulated by insulin. [97] Glomerulus extracts glucose which is then released back into circulation at the proximal tubule. To capture this specific flow, it is modeled that glucose enters the kidneys directly from the arteries (the heart compartment) and then the membrane gradient transport represents the proximal tubule glucose release. Only the glucose that is directly produced from gluconeogenesis or utilized by the kidneys is modeled. Apart from these changes, the flows and reactions follow the standard scheme.

The basal kidney glucose uptake was measured by Meyer et al. to be circa 20 mg/min and basal glucose release to be 29 mg/min. [57] Kidney glycogen stores are limited [51] and are omitted from the model. From rat data it can be estimated that the kidney oxidates circa 80 μmol/h/g dry tissue [73]. If we assume the kidneys to have 290 grams [96] and the dry to wet ratio to be 0.2, then that is circa 14 mg/min of glucose oxidation. Data from Meyer et al. [57] also show that glutamine is produced at a rate of circa 2 mg/min and glutamate is netly released also at a rate of circa 2 mg/min, both in glucose equivalents. It is assumed that the source of these flows is the uptaken glucose. That would leave 2 mg/min unexplained which are modeled to be released as lactate. The main gluconeogenic substrates are lactate (50%), glutamine (20%) and glycerol (10%). In the model, other minor substrates which are not modeled are assumed to be amino acids. Since renal glucose release is measured to be 29 mg/min [57], that is 14.5 mg/min of lactate, 11.6 mg/min of amino acid and 2.9 mg/min of glycerol net inflow. It is assumed that the hexokinase parameters K_m and K_i are the same as in the liver and also that the glucose and G6P concentrations are the same. From these parameters and basal rates, maximum velocities for hexokinase and glucose to G6P reactions are calculated.

The insulin effect

Meyer et al. [57] and Cersosimo et al. [16] measured kidney glucose uptake and release during a hyperinsulemic euglycemic clamp in humans. Meyer used the insulin infusion rate of 6.0 mU/kg/min, Cersosimo 0.25 and 0.125 mU/kg/min as high and low infusion experiments. In the experiment by Meyer et al., insulin levels stabilized at 6.8-fold of basal levels and reduced glucose production to circa 0.4 of basal rates, and increased glucose uptake to circa 1.3 of basal rates. In the measurements of Cersosimo et al. the high infusion raised insulin levels to circa 2.8 of basal levels, increased renal glucose uptake 1.9 times and decreased glucose production to 0.48 of basal

levels. The low infusion raised insulin levels 1.4 times, and increased renal glucose uptake 1.7 times and decreased glucose production to 0.6 of basal levels. While the effects on gluconeogenesis agree, Meyer et al. measured lesser glucose utilization for higher normalized insulin levels than Cersosimo et al. Generally, it seems from the data that insulin stimulation of uptake is in the range of 1.3 to 2 of the basal uptake. It is assumed that insulin can raise glucose utilization 1.5 at saturation, 1.3 at 6.8 normalized insulin. The estimated functions for renal glucose release and glucose uptake are

$$E_{RGR}(I^N) = 0.88 + 0.5\tanh(1.2(1.2 - I^N)) \tag{3.44}$$

$$E_{RGU}(I^N) = 0.9 + 0.65\tanh(0.11I^N) \tag{3.45}$$

As indicated in an oral glucose test study [58], extra glucose utilized by the kidney seems to be primarily utilized for oxidation instead of fatty acids whose uptake is reduced. Also lactate can be oxidized in the kidney. [73] During the insulin infusion measured by Meyer et al., glutamine production and uptake did not change (4 mg/min uptake, 2 mg/min production), glycerol net uptake decreased to almost zero, lactate uptake increased to circa 23 mg/min and glutamate net release increased to circa 3 mg/min. Glucose uptake increased to circa 27.5 mg/min. Alanine stays at net 0 mg/min uptake. Since glucose production was estimated to be circa 11 mg/min [57], it is assumed that it is covered by the 4 mg/min of glutamine and the rest 7 mg/min is from lactate. Glucose is assumed to be converted to the 2 mg/min of glutamine and 3 mg/min of glutamate. That leaves 22.5 mg/min of unspecified glucose and 16 mg/min of unspecified lactate and circa 12 mg/min of amino acids. It is unclear what are the other fates of these metabolites apart from oxidation. It is therefore modeled that they are converted to pyruvate and oxidized. The saturation threshold for the conversion of pyruvate (either from glucose or lactate) is set to 50 mg/min. To estimate the insulin effects, pyruvate inflows and outflows have to be calculated first.

Arterial levels of lactate rise circa 1.3-fold when insulin rises circa 6.8-fold, where also the net lactate uptake by the kidney should be 23 mg/min [57]. For simplicity, a linear relationship between insulin levels and lactate levels is assumed. To create a sufficient gradient for such lactate inflow, pyruvate levels are assumed to drop to 0.5 of basal levels. Again, a linear decline of pyruvate is assumed with increasing insulin levels. The basal rates of PYR to LAC and LAC to PYR have to be determined to produce such lactate inflow r_{lac}. First, intracellular lactate concentration has to be found.

$$C_{out} = C_{in} - \frac{r_{lac}}{Q} \tag{3.46}$$

$$C_{cell} = C_{in} - \frac{r_{lac}}{k} \tag{3.47}$$

where C_{out} and C_{in} is outflow concentration and inflow concentration of lactate, Q is blood flow, and k is membrane transport constant for lactate. Then forming the equations to find basal rates gives:

$$2 = r^B_{pyr} C^N_{pyr} - r^B_{lac} C^N_{cell} \tag{3.48}$$

$$23 = r^B_{pyr} 0.5 C^N_{pyr} - r^B_{lac} 0.78 C^N_{cell} \tag{3.49}$$

where r^B_{pyr} and r^B_{lac} are the basal rates of pyruvate to lactate, and reverse reactions. It might be surprising that the intracellular lactate levels drop in the second equation even when arterial lactate increases. This is necessary to create a sufficient gradient to achieve the measured lactate uptake by Meyer et al. Solving the equations yields: $r^B_{pyr} = 48.7$ mg/min, $r^B_{lac} = 60.7$ mg/min.

Arterial levels of amino acids decrease or stay the same during insulin stimulation [57]. Since pyruvate levels are modeled to drop, both the conversion of pyruvate to amino acids and the other way around will decrease. This is assumed to cause no significant changes in net amino acid inflow; the net inflow stays at 8 mg/min.

Net glycolysis (glycolysis - gluconeogenesis) can be calculated to find net G3P to PYR flow. The difference between $r^B_{RGU} E_{RGU}$ and $r^B_{RGR} E_{RGR}$ (net uptake) equals the net glycolysis, where r^B_{RGU} is basal renal glucose uptake and r^B_{RGR} is basal renal glucose release. Now the rate of pyruvate oxidation can be calculated by adding inflow of lactate, amino acids, and net glycolysis rate. After normalizing the calculated oxidation rates by the basal rate, the insulin effect on PYR to ACoA is found

$$E_{oxid}(I^N) = 1 + 6.89 \tanh(0.24(I^N - 1)) \tag{3.50}$$

Insulin's effect on PEPCK [75] is modeled to provide for the reduction in gluconeogenesis (PYR to G3P), while G3P levels are assumed to stay constant. Net uptake must equal net G3P to PYR flow at steady state.

$$r_{RGR} - r_{RGU} = 29 E_{gng}(I^N) - 20 \tag{3.51}$$

The calculated data showed slightly negative (-1 mg/min) rates for PYR to G3P at 8-fold insulin level rise. To produce physiologically plausible results, it is assumed that at this insulin level the rate is 0.5 mg/min.

$$E_{gng}(I^N) = 1.06 - 1 \tanh(0.45(I^N - 0.87)) \tag{3.52}$$

To keep the G3P levels constant, the G6P to G3P flow has to balance out all the other flows. Glycerol inflow is reduced with the same function that is used to reduce lipolysis in the adipose tissue.

$$E_{glc}(I^N) = 1.13 - 0.63 \tanh(0.71(I^N - 0.71)) \tag{3.53}$$

Because no insulin effect is assumed on the G6P to G3P the modulation is preformed by G6P levels. Again, net G6P to G3P flow has to equal net glucose uptake.

$$r_{RGR} - r_{RGU} = 29 - 20C_{g6p}^{N} \tag{3.54}$$

Before calculating insulin's effect on G6Pase [75] (G6P to GLU), we need to find the renal intracellular glucose concentration. After insulin levels rise, the kidney glucose release decreases. To achieve that in the model, kidney glucose levels have to decrease to reduce the gradient outflow.

$$r_{RGR} = r^{B} E_{RGR} \tag{3.55}$$

$$C_{out} = C_{in} - \frac{r_R GR}{Q} \tag{3.56}$$

Where r is the outflow of glucose and Q is the kidney output blood flow for glucose. For a stable state, the flow r_{RGR} has to equal membrane transfer to the cell.

$$C_{cell} = C_{out} - \frac{r_{RGR}}{k} \tag{3.57}$$

Where C_{cell} is the glucose concentration in the cells, k is the glucose membrane transport constant. The change in kidney intracellular glucose levels affects the activity of hexokinase which is modeled as insulin-independent. G6Pase activity with hexokinase and glucose inflow from glomerulus has to produce net outflow r. Since we know both intracellular glucose and G6P concentrations, inflow and outflow of glucose and hexokinase rate, we can calculate the effect of insulin on G6Pase. When attempting to do so, the results produce negative flows for hexokinase. This is mainly because hexokinase is inhibited by higher G6P levels and cannot produce the calculated net uptake even if G6Pase would be completely inhibited. To correct this, it is assumed that insulin also affects hexokinase. The effect is split in half between hexokinase and G6Pase to achieve the predicted flows.

$$E_{G6Pase}(I^N) = 5.22 - 4.79 \tanh(0.77(I^N + 0.81)) \tag{3.58}$$

$$E_{hk}(I^N) = 2.13 + 2.11 \tanh(0.55(C155 - 2.09)) \tag{3.59}$$

where E_{hk} is the effect of insulin on hexokinase.

3.2.5 Gut and non-liver abdominal organs

Sorensen modeled the Gut compartement as having an uptake rate of 20 mg/min which is insensitive to changes in glucose or hormonal levels. The Gut block contains the gut, spleen and pancreas. The main metabolic fuels for the gut are glutamine and ketone bodies, while glucose gets mainly converted to lactate and alanine. Rat studies of small intestine show that only circa

10% of taken up glucose is oxidized ([80], p. 125). The small intestine is capable of gluconeogenesis but that is not visible during fasting but rather during prolonged starvation, at least in rat models. [60] The gluconeogenesis of gut is not taken into account in the model and Sorensen's assumption are used. If we follow the rat data for oxidation of glucose, that would result in 2 mg/min of glucose. To balance out whole body lactate inflows and outflows, lactate release is assumed to be 7 mg/min and 11 mg/min is then assumed to leave the Gut block as amino-acids.

3.2.6 Adipose tissue

Adipose tissue maintains plasma fatty-acid levels through lipolysis of its large lipid stores. It is sensitive to insulin which can increase glucose uptake and also inhibit lipolysis. [21] Sorensen does not model adipose tissue separately but includes it in his Periphery module.

Basal flow rates
Glucose can be oxidized, turned to a lipid, be turned into glycerol [50] or leave the cell as lactate. The primary energy source for adipose tissue is glucose catabolism, with lactate release being circa 20% of the glucose uptaken [25]. Lipid synthesis from glucose is possible but is of very small magnitude ([80] 57) and is not considered in the model. Wolfe et al. measured the rate of appearance of glycerol at rest to be 2.1 μmol/kg/min and that 20% of the released free fatty acids get reesterified in the cell [95]. If we assume that all of the 20% reesterified fatty acids needs the glycerol-3-phosphate to be replaced from glucose then that is circa 29.4 μmol/min of glycerol, or in glucose equivalents 2.6 mg/min, for the model 3 mg/min. Mitrou et al. measured basal adipose tissue uptake in women from forearm to be 0.55 μmol/100 ml tissue/min. [61] Fat is circa 0.9 g/ml and Sorensen assumes adipose tissue to have 10 kg (Sorensen, 59). That gives 11 mg/min glucose uptake. If we assume that 20% of lactate leaves the adipose tissue, that gives 2.2 mg/min and leaves $11 - 2.2 - 2.6 = 6.2$ mg/min for oxidation, for the model 6 mg/min. With 4 kcal/g of glucose oxidation that should produce 0.025 kcal/min. With the adipose tissue having resting energy expenditure of 0.031 kcal/min [96] that seems reasonable. The parameters of hexokinase and concentrations of glucose and glucose-6-phosphate are assumed to be the same as in the muscle. The lactate to pyruvate reaction is assumed to be 10 mg/min and pyruvate to lactate reaction 12 mg/min.

The effect of insulin

Insulin stimulates glucose uptake in adipose tissue through GLUT4 translocation [21] but it is assumed no other glucose-related pathways are stimulated by insulin. In vitro data of glucose uptake during insulin stimulation resemble GLUT4 kinetics [48]. However, when attempting to calculate the flows under these assumptions, the G6P levels were high, inhibited hexokinase and glucose was not able to stimulate the hexokinase enzyme enough. For that, it is assumed that both hexokinase and G6P to G3P are insulin stimulated, while their concentrations stay at basal levels; the same scenario as in skeletal muscle. Virtanen et al. measured uptake in adipose tissue during insulin infusion which increased insulin levels 13.2-fold compared to basal levels. From their study, adipose tissue uptake was estimated at 45 mg/min at that insulin level [91]. The shape of the insulin effect function on glucose uptake is the same as the one used in the muscle section when estimating adipose glucose uptake.

$$E_{uptake}(I^N) = 2.75 + 1.75 \tanh(0.5(I^N - 5.5)) \tag{3.60}$$

Having the uptake under insulin stimulation r_{upt}, the effect of insulin on GLUT4 translocation can be calculated

$$C_{out} = C_{in} - \frac{r_{upt}}{Q} \tag{3.61}$$

where C_{out} is the vessel outflow concentration of glucose and Q is the input blood flow. Then the E_{glut4} can be calculated from

$$r_{upt} = E_{glut4} k (C_{out} - C_{cell}) \tag{3.62}$$

$$E_{glut4}(I^N) = 3.1 + 2.14 \tanh(0.49(I^N - 5.61)) \tag{3.63}$$

where k is the membrane transport constant and C_{cell} is intracellular glucose concentration, which is known. The glucose to G6P and G6P to G3P reactions are stimulated with the function E_{uptake}.

The conversion of glycerol to G3P is modeled to depend on lipolysis, which is inhibited by insulin. A study by Moberg et al. [62] on glycerol release during insulin stimulation and euglycemic clamp found that compared to basal levels, glycerol release from adipose tissue drops to circa 0.55 at circa 3 times insulin rise and saturates at 0.5 at 19-fold increase. These points were fitted to estimate the effect of insulin on glycerol release/lipolysis.

$$E_{lipo}(I^N) = 1.13 - 0.63 \tanh(0.71(I^N - 0.71)) \tag{3.64}$$

It is assumed that G3P conversion to glycerol is affected by the same function. With reduced lipolysis it is assumed that glucose oxidation saturates as insulin rises. The resting energy requirements at 0.031 kcal/min would require circa 8 mg/min of glucose. This is approximated by the function

$$E_{oxid}(I^N) = 0.5 + 0.85 \tanh(0.67 I^N) \tag{3.65}$$

3.2.7 Skeletal muscle

Skeletal muscle is modeled in Sorensen as a part of the Periphery block incorporating skeletal muscle and adipose tissue. Since Sorensen provides only a combined glucose uptake metrics for this Periphery tissue block, it is necessary to ascribe consumption to individual tissues.

Initially, the skeletal muscle compartment was modeled as having a combined equilibrium space and interstitial space. However, when running simulations for intravenous glucose tolerance tests, it showed important to have this separation, even though the glucose transport constant for vessel membrane transport estimated by Sorensen is relatively small (5 min). Sorensen compared his model performance with venous samples from peripheral circulation, which had a characteristic blunted response compared to the arterial glucose and insulin levels. Adding the membrane assured the correct curve type and also provided a more realistic physiological model. Nevertheless, the extra membrane was not added to the adipose tissue because its volume and blood flow is comparatively smaller than the muscles' and hence it can be simplified.

Basal flow rates

Sorensen assumes muscle to have 30 kg. However, in a study Janssen et al. measured the skeletal muscle mass of men to be 38.% of total body mass [40], which for a 70 kg man would be 26.88 kg. The model assumes muscle mass to be 27 kg. In a study of Kelley et al. measured basal forearm muscle uptake to be circa 23.1 mg/min [45] and Meyer et al. measured basal forearm muscle uptake to be 24.1 mg/min [58]. In a different study, Kelley et al. measured skeletal muscle uptake from femoral muscle and measured it to be 7.2 mg/min [45]. A simple average of forearm and femoral muscle uptake yields circa 15 mg/min which is used in the model. The basal oxidation of glucose can be determined through resting energy expenditure. The skeletal muscle has a metabolic rate of 13 kcal/kg tissue/day [96], or 0.244 kcal/min. Under normal conditions, skeletal muscle uses ketones for less than 5% of energy provision, 10% after overnight fast [24]. If we assume it to be 5% then that is 0.012 kcal/min. Van Hall et al. in a study [88] measured femoral muscle fatty acid oxidation to be 16 μmol/min. If we assume the oxidised fatty acid to be the palmitic acid, which is the most common in the body [15], then that is 4.1 mg/min. Van Hall et al. assume the femoral muscle to be 5 kg, hence extrapolating to the whole body gives 22.1 mg/min. With energy release of 9 kcal per gram of fatty acid oxidation, then that gives 0.199 kcal/min. 0.244 - 0.199 - 0.012 = 0.033 kcal/min. If we assume 4 kcal/g for glucose oxidation, that means circa 8.2 mg/min of glucose oxidation. Since we have seen that femoral and forearm glucose uptake differs it has to be taken with limitation whether this glucose oxidation is a valid average for the whole body. Kelley et al. measured basal glucose oxidation to be 8.7 mg/min, based on femoral muscle measurements. In a review, Frayn estimates whole-body skeletal muscle fatty acid utilization to be 20.8 mg/min (converted from day to minutes) [26], which would make the resulting glucose oxidation slightly higher. For the model, it is assumed that glucose is oxidized at a rate of 9

mg/min in a basal state.

At rest, muscle releases lactate netly, estimated to be circa 11 mg/min [89]. To compensate for the difference between the uptake and lactate/oxidation requirements, glycogen stores are utilized as was observed in the study of Kelley et al. [45]. For the model, the basal net glycogenolysis is assumed to be 11+9-15=5 mg/min.

The insulin effect

After glucose enters the cell, it is converted to glucose-6-phosphate through the enzyme hexokinase. Heart hexokinase has Km of 0.1 mmol/l [43]. Furthermore, in the brain, the inhibitory constant K_i of G6P on hexokinase is circa 0.2 mmol/l [86] If we assume the same values for skeletal muscle, and 0.5 mmol/l glucose and 0.13 mmol/l G6P concentrations [71], then normalized constants would circa be, $K_m = 0.2$, $K_i = 1.5$. Maximum rate is then calculated to fit with the basal uptake of glucose (15 mg/min), $v_{max} = 30$ mg/min. This combination of saturable conversion of glucose and inhibition by the product produces a non-linear relationship. This is in contrast with Sorensen, who models glucose uptake as a one-to-one linear function dependent on interstitial muscle glucose concentration ([80], p. 68). By doing this he possibly overestimated the effect of glucose concentration and the effect of insulin on uptake should be corrected in this way.

From the data compiled by Sorensen, the normalized peripheral interstitial glucose concentration is available. For conversion to mg/dl, basal interstitial glucose concentration was calculated (for equations see Initialization of the model) and multiplied by the normalized value. The goal is to calculate the rate r of glucose uptake at such interstitial glucose levels, without the effect of insulin. This rate was found from the following equations at steady state:

$$r = k(C_{inter} - C_{cell}) \tag{3.66}$$

$$r = 30 \frac{C^N_{cell}}{0.2 + C^N_{cell}} \frac{1}{1 + \frac{C^N_{g6p}}{1.5}} \tag{3.67}$$

$$r = 150 \cdot C^N_{g6p} + 20 \cdot C^N_{g6p} - 155 \tag{3.68}$$

The first equation is the interstitium-cell membrane transport, k is the membrane constant. The second equation is the hexokinase reaction, where C^N_{cell} is normalized intracellular glucose concentration and C^N_{g6p} is normalized G6P concentration. The last equation is the balance of flows of the G6P metabolite. Since we have three equations and three unknowns (C^N_{cell}, C^N_{g6p}, r) we can solve them. After that, the found r is normalized by the basal rate $r_B = 15$. Sorensen in his data provides the normalized rates of peripheral glucose uptakes which include both the effect of insulin and glucose. Glucose uptake with only insulin effect is found:

$$r^N_I = \frac{r^N}{r^N_G} \tag{3.69}$$

where r^N is the normalized peripheral glucose uptake reported by Sorensen, r_G^N is the normalized peripheral glucose uptake rate that would be caused only by glucose levels, and r_I^N is the uptake caused only by interstitial insulin.

Having found only the effect of insulin, it is possible now to estimate a new function of insulin effect on the peripheral glucose uptake. A 34 mg/min basal uptake is assumed to convert the uptake rates from normalized to mg/min. Next, a separation of the adipose tissue uptake is needed. An approximation of adipose insulin effect was constructed based on assuming 10 mg/min basal uptake and circa 45 mg/min as a maximum response to insulin. The value is for 13.2-fold basal insulin increase and was estimated from measurements of different types of fat tissues [91]. The following function was used:

$$E_A(I^N) = 2.75 + 1.75 \tanh(0.5(I^N - 5.5)) \tag{3.70}$$

where I^N is the normalized peripheral interstitial insulin and the uptake rates were found as $r_A = E_A \cdot 10$, and subtracted from the peripheral uptake rates. The remainder now represents forearm muscle uptake (since all the above data provided from Sorensen come from forearm studies). The rates in mg/min are divided by 24 mg/min to obtain normalized forearm muscle uptake. A curve is estimated to fit the muscle normalized uptake rates.

$$E_{FMGU}(I^N) = 7.5 + 6.8 \tanh(0.6(I^N - 4.15)) \tag{3.71}$$

where $E_{FMGU}(I^N)$ is the effect on insulin on forearm muscle uptake.

The next task is to accommodate the forearm muscle uptake with femoral muscle uptake. For 6.8 normalized insulin, Kelley et al. measured 150 mg/min basal uptake at femoral muscle, whereas the fitted forearm function predicted 330 mg/min [45]. For 13.2 normalized insulin Virtanen et al. measured 272 mg/min for femoral muscle, fitted forearm function predicted 343 mg/min [91]. Following the same assumption of taking a simple average as with the basal uptake rates, averages were taken, and divided by the basal uptake (15 mg/min) for normalization. To fully fit a tanh function with four parameters, at least four points are needed. From preliminary model testing on intravenous glucose tolerance tests, it seems that a sharp rise in glucose uptake is necessary even if interstitial levels of insulin do not rise as much. To provide for that, the fourth point is modeled to pass through the point [0,0] even though theoretically at zero insulin levels there should still be some uptake. These four values were then used to fit an tanh function which would approximate the dependency of glucose uptake on normalized muscle insulin. The important thing is that this new function should be more representative of the whole body skeletal muscle.

$$E_{MGU}(I^N) = 9.69 + 11.02 \tanh(0.3(I^N - 4.56)) \tag{3.72}$$

The function was estimated using the python scipy.optimize library function curve_fit. The determined uptake flow then splits between lactate production, oxidation and storage as glycogen.

Insulin stimulates GLUT4 translocation, hexokinase activity and phosphofructokinase activity (glycolysis). It also stimulates glycogen synthesis and suppresses glycogenolysis. Rat muscle measurements show that G6P and glucose levels don't rise under insulin stimulation suggesting the influence of insulin on glucose-processing enzymes. [21] However, this increased enzymatic activity does not result in a significantly greater net lactate release ([80], 57), [45], which is also why lactate outflow is assumed as constant under euglycemic insulin stimulation. In the model, glycogen synthesis and breakdown are equally affected by insulin to produce net glycogen flows. These can be determined after determining the influence of insulin on the oxidation of glucose.

Sorensen cites a study showing that glucose oxidation did not significantly increase after a 100 gram oral glucose tolerance test (OGTT), concluding that oxidation is not a significant route of glucose disposal ([80], p. 57). However, Kelley et al. showed that insulin infusion during an euglycemic clamp increased glucose oxidation nearly six times its basal rate. [45]. Glucose oxidation is regulated among others by fatty acid availability. [21] The difference could be possibly caused by the delays in fatty acid signalling which, for a full effect, needs to reach the muscle after being first suppressed by insulin in the adipose tissue. The study of Kelley et al. shows that glucose uptake reaches full saturation only after circa 150 minutes, so it could be possible that the fuel metabolism does not switch that quickly after an oral glucose test. The effect is nonetheless limited – only so much fatty acid oxidation can be replaced. In the cardiac muscle, after insulin stimulation, 60-70% of the cardiac energy metabolism can be provided by glucose oxidation [38], where as at rest (without insulin stimulation) 70% is provided by fatty acid oxidation. [55]. In the study of Kelley, fatty acid oxidation dropped practically to zero (0.1+-0.2 μmol/100 ml tissue/min) after insulin stimulation and euglycemia. For the model, it is assumed, that glucose can cover at most 80% of the resting skeletal muscle energetic needs, or 0.195 kcal/min, oxidating circa 50 mg/min. It is assumed that the effect rises linearly with normalized muscle insulin concentration, up until saturation:

$$E_{oxid}(I^N) = 5.55 \tanh(0.183 I^N) \tag{3.73}$$

Net glycogen flow dependence on insulin can be calculated as the difference between total uptake and glycolysis (oxidation, lactate release). After that, the difference is divided by two and the rates of glycogen synthesis and glycogenolysis are calculated. From the resulting data, curves are estimated

$$E_{g\_syn}(I^N) = 1.39 + 0.46 \tanh(0.33(I^N - 4.85)) \tag{3.74}$$

$$E_{g\_lys}(I^N) = 0.62 + 0.44 \tanh(-0.33(C108 - 4.84)) \tag{3.75}$$

where E_{g_syn} is insulin effect on glycogen synthesis and E_{g_lys} is the insulin effect on glycogenolysis. G6P to G3P stimulation is calculated as the sum of

lactate production (constant) and oxidation, assuming constant G6P levels based discussion above. A curve is estimated:

$$E_{g6p-to-g3p}(I^N) = 0.28 + 2.79 \tanh(0.17(I^N + 0.54)) \tag{3.76}$$

The effect of insulin on GLUT4 translocation has to be estimated also, because with increasing uptake rate, the interstitial concentration of glucose falls to create a gradient. However, this decreases the gradient to cell, because intracellular glucose concentration is assumed constant (as discussed above). The interstitial concentration can be calculated from vessel outflow concentration since we are calculating in an euglycemic state.

$$C_{interst} = C_{out} - \frac{r}{k_1} \tag{3.77}$$

$$C_{out} = C_{in} - \frac{r}{Q} \tag{3.78}$$

where $C_{interst}$ is interstitial concentration, C_{out} is vessel outflow concentration, C_{in} is inflow concentration, both for glucose. k_1 is vessel-interstitium membrane constant. The effect of insulin is then:

$$r = E(I^N)k_2(C_{interst} - C_{cell}) \tag{3.79}$$

where k_2 is the interstitium-cell membrane constant, C_{cell} is intracellular concentration and r is the calculated uptake. A curve for the insulin effect on cellular glucose membrane transport is estimated:

$$E_{glut4}(I^N) = 24.17 + 25.41 \tanh(0.3(I^N - 6.13)) \tag{3.80}$$

3.2.8 Other tissues

The lungs compartment is joined with the heart in the work of Sorensen, but no lung glucose uptake is estimated – it is implicitly a part of the Periphery block. Sorensen estimated red blood cell uptake to be 10 mg/min at a constant rate, insensitive to glucose, insulin or glucagon levels. ([80], p. 48, 51) Furthermore, in vitro data suggest that circa 90% of the uptaken glucose leaves the cell as lactate [39], so in the model 9 mg/min of lactate is released from red blood cells.

O'Neil et al. measured glucose uptake in the rat perfused lungs, and found the uptake rate of 11.2 μmol of glucose per gram of tissue per hour. The authors assume half of this value for humans, since the human lung consumes half of oxygen compared to the rat lung. Furthermore, half of the uptaken glucose is released as lactate [68]. Mean weight of the human lungs is 840 grams [63], which would give circa 14 mg/min of glucose uptake. Both red blood cells and the lungs are modeled as simple sinks and sources without the full organ structure. They are connected directly to the heart module.

Kraegen et al. measured that rat lung tissue is sensitive to insulin and stimulates glucose uptake. [47] A function is estimated from the data

$$E(I^N) = 2.01 \tanh(0.56 I^N) \tag{3.81}$$

where I^N is the normalized insulin concentration at heart.

3.3 Insulin clearance and release

The insulin release and clearance are modeled according to Sorensen. The only difference is in the peripheral compartment, which is separated into muscle and adipose tissue in this model. Sorensen modeled a membrane between the equilibration space and the interstitial space, which is also modeled for the skeletal muscle. The insulin clearance from the peripheral interstitial compartment is calculated as ([80], p. 219)

$$K = \frac{1 - 0.15}{0.15} \frac{1}{Q} - \frac{20}{V} \tag{3.82}$$

$$r_{IC} = \frac{C_I}{K} \tag{3.83}$$

where K is a clearance constant, 0.15 is the fractional extraction, Q is blood flow (for insulin), 20 is the time constant for insulin membrane transport [min] and V is interstitial volume. After inputting the estimated values of blood flow and interstitial volume for muscle, a value of $K = 3.06$ was obtained. r_{IC} is the rate of muscle insulin clearance [mU/min] and C_I is the concentration of muscle interstitial insulin. The adipose tissue produced negative clearance values with this approach and therefore a simpler way was selected. The adipose tissue has relatively small volumes and is not a significant tissue of glucose clearance, it should be then sound to combine the equilibrium and interstitial volumes and set the insulin clearance rate directly to 15% of the incoming insulin mass flow.

Adipose tissue, liver and kidneys clear insulin based on the equation

$$r_{IC} = C_{IH} Q F \tag{3.84}$$

where C_{IH} is the insulin concentration from the inflowing organ - heart, Q is the blood flow for insulin and F is the fractional clearance for each tissue, for kidneys = 0.3, liver = 0.4, adipose tissue = 0.15.

Insulin release is taken directly as modeled in Sorensen, without any changes and connected to the liver as in his model. For a list of his equations on pancreatic insulin release please see ([80], p. 219-220).

3.4 Modeling glucose intolerance

As Sorensen discusses, the reaction to an intravenous glucose test can vary significantly even for persons with the same medical diagnosis (namely, type

1 diabetes mellitus). Furthermore, antibodies binding insulin in plasma may delay insulin dynamics (although this shouldn't be an issue with purified insulins), and glucagon response can be diminished. A whole range of models can be constructed ([80], p. 356-357). Since Sorensen decided to use the model for therapy development purposes, he set the pancreatic insulin response to zero and left everything else the same as in the typical metabolism. In other cases of glucose intolerance, the insulin response is typical or higher, but the intolerance is caused by tissue insulin resistance. This is caused by either receptor or post-receptor resistance ([80], p. 318).

For modeling, the general effect of insulin production, and two types of resistance were picked. The pure receptor resistance is characterized by achieving the same insulin response as in a typical metabolism, yet only with higher than typical insulin levels. This could be modeled as:

$$E_{inhib}(I^N) = 0.5[1 + A\tanh(B(I^N - C))]E(I^N) \tag{3.85}$$

where $E(I^N)$ is the typical tissue insulin response and tanh is the resistance effect. The pure receptor response is simulated by changing the C parameter - if the C parameter is set to a large positive number, the normalized insulin concentration has to rise proportionately to achieve the same maximum response. The post-receptor resistance decreases the maximum response, meaning that even for large insulin concentrations, the response saturates below the typical maximum response. This is modeled by decreasing the term A below one, but above zero (no response). B is set to 0.5 to provide a more smooth transition.

This approach can not be used for glycogenolysis. Insulin normally suppresses glycogenolysis and in case of insulin resistance fails to do so. Applying such a function for insulin resistance to liver glycogenolysis would suppress it already in the basal state which would inhibit it and the glucose circulation system would collapse. Hence a simple way is used to model insulin resistance in glycogenolysis, and that is adding an S parameter directly to the insulin effect tanh function, which can right-shift the insulin-dependence curve. The following equation shows the principle.

$$E_{break}(I^N) = 1.0 - 1.0\tanh(1.0(I^N - 1.0 - S)) \tag{3.86}$$

3.5 Initialization of the model

The initialization of the model is taken from Sorensen ([80], p. 264-265). The heart module is initialized with the concentrations described in the basal concentrations section; glucose - 97.3 mg/dl, lactate 10.7 mg/dl, glycerol 0.7 mg/dl, 4.6 mg/dl, insulin 1.5 mU/dl. First, the initialization of non-insulin metabolite concentrations is described. For each tissue, the basal extracellular concentration (or equilibrium space concentration for muscle) was calculated as

$$C_{out} = C_{in} - \frac{r}{Q} \tag{3.87}$$

Where C_{out} is the output extracellular concentration, r is the net inflow of a metabolite (negative for outflow) and Q is the output blood flow. C_{in} is the mixed input concentration from input organs.

For muscle, the interstitial concentration was calculated in a similar way

$$C_{interst} = C_{out} - \frac{r}{k} \tag{3.88}$$

Where k is the vessel-interstitium membrane constant.

The calculations for insulin are the following. If the tissue has no insulin clearance (brain, gut, lungs, RBC and heart), then its initial concentration is the same as in the heart compartment. Adipose tissue and kidneys have initial concentrations

$$C_{out} = C_{in}(1 - F) \tag{3.89}$$

where C_{in} is input insulin concentration (heart) and F is the fractional clearance constant.

For the liver, an equation using the mass conservation of insulin loop is used.

$$Q_L I_L = H - B - K - M - A; \tag{3.90}$$

Where H is the heart insulin output mass flow, similarly then B, K, M, A are brain, kidneys, muscle and adipose tissue insulin output mass flows. Q_L is liver insulin output blood flow. After liver insulin concentration is found, the basal pancreas insulin release can be calculated:

$$r = \frac{Q_L}{1 - F_L} I_L - Q_G I_G - Q_A I_H \tag{3.91}$$

where r is the basal pancreas insulin release in mU/min, Q_L is the liver insulin output blood flow, Q_G and Q_A are input blood flows for insulin from the arteries and the gut into the liver, I_G and I_H are gut and heart insulin concentrations, and F_L is liver insulin fractional clearance.

Glucagon is set to 80 pg/ml, following the data from the study of Meyer et al. [57].

3.6 Implementation in Modelica

To allow for maintainable development, a modular approach was selected. The general idea was to have a standard module for a tissue, that would be consecutively specialized. Having a standardized tissue module could prove to be limiting if one would like to develop a very detailed physiological model of a certain tissue while keeping others the same. To be physically consistent, all metabolites are modeled as masses and not concentrations, as would be

typical for most models. This allows for truly conserved flows since mass is a conserved quantity. Metabolite flows in the literature are often reported in minutes and Sorensen's model uses minutes too. Since Modelica's derivations use seconds as a time unit, a conversion is necessary to form a mass flow per minute.

3.6.1 Base tissue

In the base tissue model `TissueModel`, there are no reactions, only three metabolite pools and a system of exchange with blood flow. Metabolites in the transfer pool `TransPool` represent intracellular metabolites that can leave the cell, and metabolites locked inside the cell are in the `LockedPool`. The reason for this division is that the metabolites which come into exchange with plasma/interstitium can be expressed directly as a vector instead of individual description. A third pool is the extracellular pool `ExtraPool`, which contains the metabolites in the extracellular space. The `RealInput` is prepared to be connected to the input organ concentration variable and is used to calculate input mass flow. The output mass flow is based on `ExtraPool` metabolite concentration and output blood flow. The input mass flow and output mass flows are calculated according to equations in the subsection Metabolite circulation. The metabolite input mass flow and output mass flow are expressed as a metabolic source and sink and connected to the `ExtraPool`. The membrane transport is modeled according to the equation in Metabolite circulation. Insulin from `ExtraPool` does not enter the cells and therefore a middle-step connector with only exchangeable metabolites is used. By default, this middle-step connector is connected to the membrane module and the transfer pool is connected to it. The middle-step connector can be disconnected by setting the `combined` parameter to false, which is used in the skeletal muscle module to add another membrane. In total, the base tissue model `TissueModel` creates a hollow shell with metabolite pools and mass inflow and outflow.

3.6.2 Glycolytic tissue

The modeled organs can be divided into two categories - those who only perform glycolysis and those who besides it can also perform gluconeogenesis. Glycolysis is a feature common to all modeled organs and therefore was selected as the second inheritance step. The model for a glycolytic tissue inherits from the module `TissueModel` and adds glycolytic reactions to it. These are: glu-to-g6p, g6p-to-g3p, g3p-to-pyr, pyr-to-lac, lac-to-pyr, pyr-to-acoa, acoa-sink. The reactions are described in the section Intracellular reactions.

The intracellular reactions contain an input metabolite and an output metabolite. Every reaction is driven by the input metabolite mass and sometimes regulated by the output metabolite mass. Normalizing the mass by the basal state mass allows for using a simple way of setting up basal rates. The basal

masses are calculated from estimated or assumed concentrations and organ water volumes. The reactions are connected to the transfer pool or the locked pool depending on the metabolite. For each specialized tissue, there is a file with constants that follows an outlay shown in `GeneralConstants`. The Constants model includes volumes, blood flows, and basal concentrations for each pool. When the glycolytic tissue is specialized to a particular tissue, the `GeneralConstants` model is re-declared and replaced. The reaction rates are also specified only at the specific tissues. The tissues that directly inherit from glycolytic tissue are skeletal muscle, adipose tissue, brain, gut, and heart.

Skeletal muscle

The skeletal muscle is enlarged with a second membrane modeling the transport from equilibrium space to the interstitium. When running simulations on the intravenous glucose tolerance test without this separation, the results lacked a characteristic spike shortly after the infusion. It is also in line with Sorensen, who models his periphery compartment as having this separation. A new pool is introduced to represent the interstitial metabolite pool and the `ExtraPool` represents the equilibrium space. The membrane transport is modeled in the same way as the cell membrane transport. The extracellular pool is connected to the membrane together with the interstitial pool. This is possible directly because insulin can pass the vessel membrane. The metabolites that can be exchanged from the interstitial pool are connected to the middle-step connector. Another addition is the glycogen synthesis and breakdown reactions (gly-to-g6p, g6p-to-gly) and adding a metabolic intracellular source for amino acids (representing amino acids from muscle breakdown). The insulin clearance sink is connected to the interstitial pool.

Adipose tissue

The adipose tissue releases fatty acids through lipolysis, which is captured by adding a glycerol source, connected to the intracellular glycerol pool. For reesterification of fatty acid, a portion of glucose has to be converted to glycerol-3-phosphate which is modeled as sinking the G3P. The insulin sink is connected to the `ExtraPool`.

Gut, Heart, Brain

A pyr-to-aac reaction is added to the gut because the tissue converts glucose to amino acids. The heart and brain tissues have no changes from the `GlycolyticTissue`.

3.6.3 Gluconeogenic tissue

Modeling gluconeogenesis as a general model is useful since both the kidneys and liver are capable of gluconeogenesis. The `GlucogoneogenicTissue` inherits from the glycolytic tissue model and adds these reactions; g6p-to-glu, g3p-to-g6p, glc-to-g3p, pyr-to-g3p, aac-to-pyr, connects them to their respective pools and references the reaction metabolite basal masses to the general constant model.

Kidneys

The reaction for pyr-to-aac is added and a special connector is created for glomerular glucose uptake and is connected to the extracellular pool. This connector has to be later connected to the heart module too. The insulin sink is connected to the insulin in the extracellular pool.

Liver

Glycogen is broke down and synthesized in the liver, hence the gly-to-g6p and g6p-to-gly reactions are added. Insulin clearance is connected to the extracellular insulin pool together with insulin production source. The insulin release module is instantiated in the liver and outputs the value which drives the insulin source.

3.6.4 Regulatory effects

The regulatory effects are not modeled for all tissues, as some of them are not regulated by insulin, glucagon or glucose. These are the brain and gut tissue. For the tissues that are regulated, a division in two groups is made. First, simple tissues, namely adipose and heart tissue, have their basal rates and regulatory effects described in a single module. More complex tissues (muscle, renal and liver tissues) are composed of two modules. The first module contains the basal rates with all intracellular reactions but it does not contain any regulatory effects. The second module adds the functions for insulin, glucagon or glucose effects. This allows for simpler testing where first the basal state model is developed and then another layer of complexity is added. The tissue models without regulation effects have a `Basal` suffix in their name, for example `RenalTissueBasal`. The final tissues are called without the suffix and inherit from their basal versions. The regulatory effects are driven by normalized concentrations of intracellular (or interstitial for muscle) metabolites which affect tanh functions. The tanh functions are incorporated into the model through specifying a `reg-eff` variable present in every intracellular reaction and in the membrane transport module.

3.7 Comparison of model results to data

The model was tested on three tests which Sorensen also used to test his model. These are the intravenous glucose tolerance test (p. 269), intravenous insulin tolerance test (p. 276), and continuous insulin infusion (p. 278). The red lines represent this model's simulations which were added to the figures provided by Sorensen. Sorensen changed the basal levels for glucose and insulin depending on the experiment which was not done for this model's simulations. If a short infusion is given in the test, the dose gets delivered in three minutes. The red line in the figures is this thesis' model results, and they were all adapted from Sorensen.

3.7.1 Tests

The intravenous glucose tolerance test is shown in figure 3.3. Sorensen used this test to estimate his model parameters. From the test, it seems that the primary determinant for the different reactions is the reduced initial insulin response. The blood glucose consequently does not decrease as fast and triggers the delayed insulin release which produces the late increased venous plasma insulin levels.

Similarly to the glucose bolus, insulin can be infused. The intravenous insulin tolerance test of 0.04 U/kg (2.8 U) is displayed in figure 3.4. The plasma insulin peak is below Sorensen's results but decays a bit slower. However, the response to hyperinsulemnia is much greater than in the experimental data and Sorensen's model. Plasma glucose drops to 18 mg/dl, which probably triggers the great glucagon response which attempts to return the glucose levels to basal levels.

The continuous insulin infusion which administers 0.25 mU/kg/min (17.5 mU/min) is shown in figure 3.5. The glucose decay and stabilization are reasonably close to experimental data. However, from the experimental data on insulin infusion, it seems that insulin gets cleared by the body more quickly than in the model, which causes slower accumulation in the bloodstream.

3.7.2 Evaluation

From the tests, it seems that the metabolism (probably the muscle tissue) is too sensitive to insulin when insulin levels are very high. Under continuous insulin infusion, the glucose uptake gets also enhanced a bit too much. This is at first in contrast with the glucose tolerance test where the glucose uptake is insufficient. However, the difference is that with the glucose tolerance test, the liver insulin effects act with a delay and do not get fully mobilized. The first step to correct the model for the experimental data would be to tune the pancreas release module and insulin metabolism to achieve a correct initial insulin peak response. After that, the muscle tissue module could be reconsidered. A simple average was taken to combine the forearm muscle measurements with the femoral muscle measurements. The femoral muscle had much lower glucose uptake when extrapolated to the whole body compared to the forearm extrapolated results. More than 50% of the body muscle mass may behave more as femoral muscles than as forearm muscles. Adjusting for this should at least partially solve the severe hypoglycemia observed during the insulin tolerance test.

3.8 Structure of the web page

Glucose metabolism can be viewed for its complexity from several different dimensions. The first dimension is the organ dimension. Glucose gets produced and consumed to form a closed loop and the role of tissues and

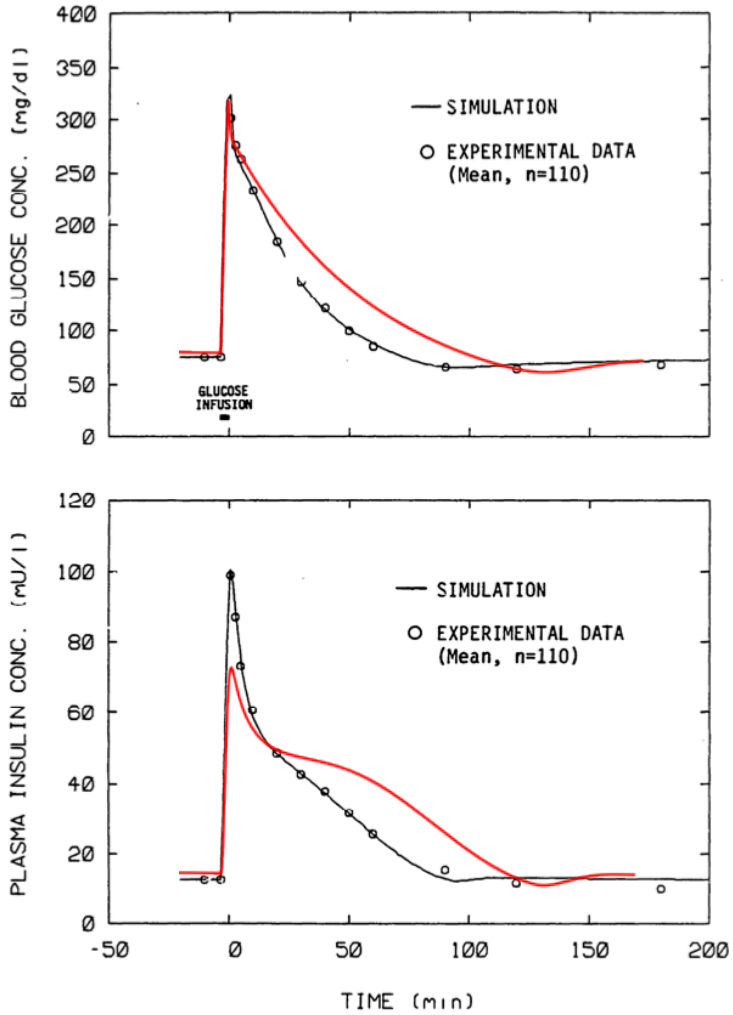

Figure 3.3: The intravenous glucose tolerance test with the dose 0.5 g/kg (35 g)

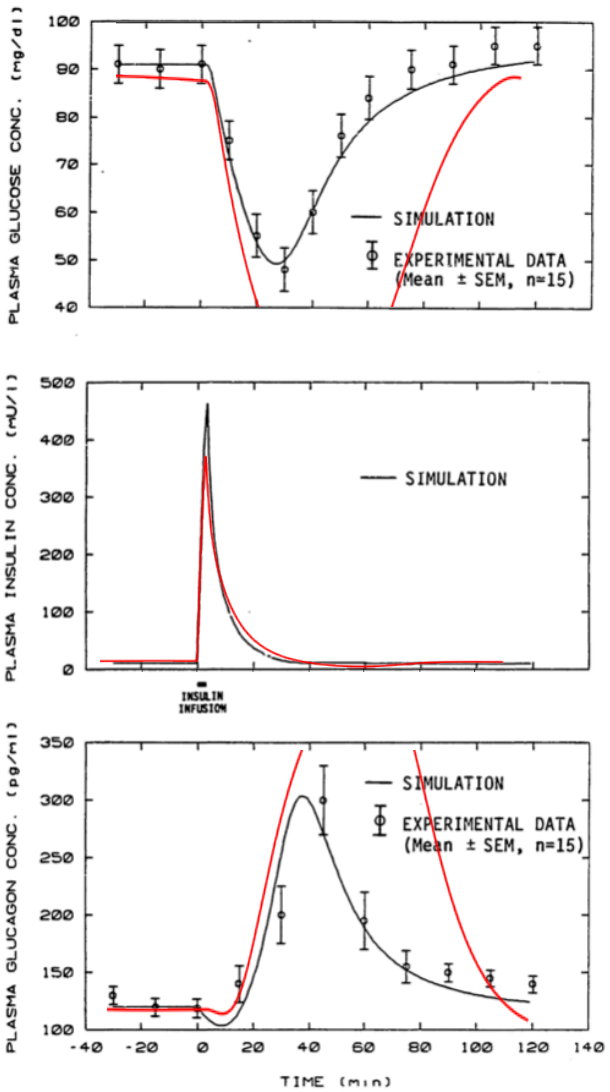

Figure 3.4: The intravenous insulin tolerance test with the dose 0.04 U/kg (2.8 U)

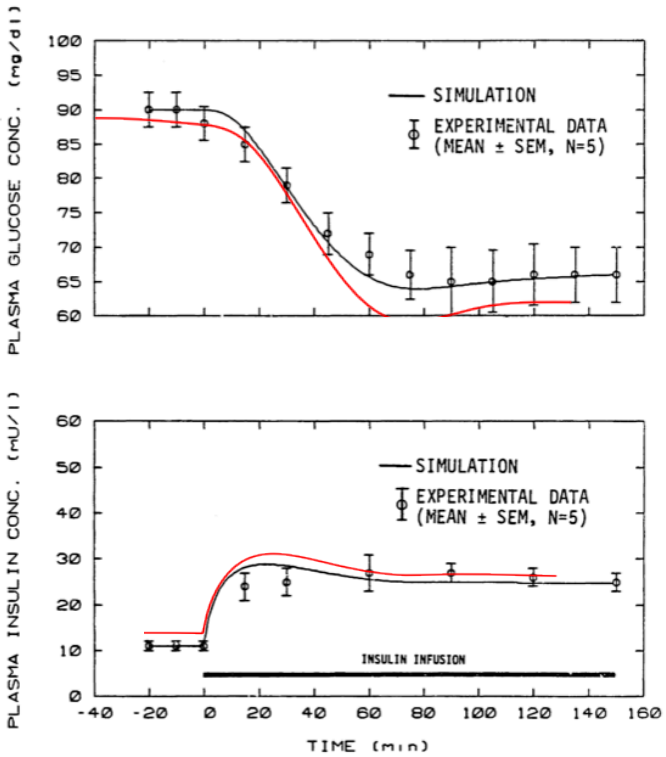

Figure 3.5: The continuous insulin infusion with the dose 0.25 mU/kg/min (17.5 mU/min)

organs can change depending on the level of glucose. The second dimension is how the net organ metabolite inflows are driven by intracellular reactions. The third is how glucose metabolism does not involve only glucose, but also lactate or amino acids and other metabolites. These metabolites are not only sources of glucose but also buffers. Fatty acids can be substituted by glucose for energetic use. The fourth dimension is regulation with the goal of homeostasis. Multiple hormones are used to react to the changing needs or consumption of glucose. Through understanding each dimension, complex glucose metabolism can begin to emerge. The concept behind the web page is to show these dimensions. The tools used for this will be graphs portraying how flows or metabolite concentrations taken from the model change in time during an experiment. The experiments will be glucose infusions where the user can set the amount of the dose. To view the dimension of regulation, modeling insulin resistance and destruction of insulin production is used. The user can set the extent of the destruction and resistance, with the possibility of creating many types of homeostasis. The graphs are complemented with texts explaining to the user the basis of the viewed process and they direct the user's attention.

The web application is chosen as a platform because of its accessibility and visualizing potential. It constitutes of three sections. The first section shows how different tissues react to a hyperglycemic state after the infusion of glucose. The second section displays lactate-glucose cycling (the Cori cycle) and through it gluconeogenesis and glycolysis. The third section shows what happens after introducing insulin resistance or reducing pancreas insulin production. The results are shown again for an intravenous glucose tolerance test.

3.8.1 Organs

The user can determine the dose of glucose that will be administered. In the first row of graphs, peripheral plasma glucose is shown on the left side and normalized insulin and glucagon peripheral plasma concentrations are shown on the right side. This offers a total overview of how the body reacts to glucose. Below that, net glucose flows for all tissues shown except the kidneys and RBCs are shown. At the bottom, liver and muscle glycogen synthesis and breakdown are displayed. Through that, the user sees where exactly the surplus glucose gets absorbed. Furthermore, they will see the role of glycogenolysis and glycogen synthesis in this process. The composition of graphs is shown in figure 3.6.

3.8.2 Metabolites and intracellular reactions

The lactate-glucose cycle (the Cori cycle) is the conversion of glucose to lactate in tissues such as muscle, adipose tissue, or the brain and its conversion back to glucose in the liver and kidneys. On top, venous glucose levels are shown. The second graph depicts the flows of glycolysis. The third graph shows

arterial lactate levels and to close the loop, the uptake of lactate by the liver is displayed in the last graph. The composite view of these flows should allow the user to see how the production of lactate through glycolysis in one tissue drives lactate levels, which affect gluconeogenesis. For the outlay on the web page see figure 3.7.

3.8.3 Glucose intolerance (Regulation dimension)

In this section, the user can change the parameters of the metabolism and administer a fixed dose of 35 g of glucose. The first is the insensitivity of the liver glycogenolysis to insulin, the second is the capacity of the pancreas to produce insulin. The third is the insensitivity of muscle glycogenolysis to insulin, the fourth and fifth produce the insensitivity of muscle uptake and reduce the maximum effect of insulin. For comparison, changed metabolism is shown on the left side and typical metabolism is on the right. In the first row of graphs liver glycogenolysis is shown. In the second, muscle glycogen breakdown and glucose uptake is displayed. In the third, venous glucose and insulin levels are shown (normalized) to give a global overview.

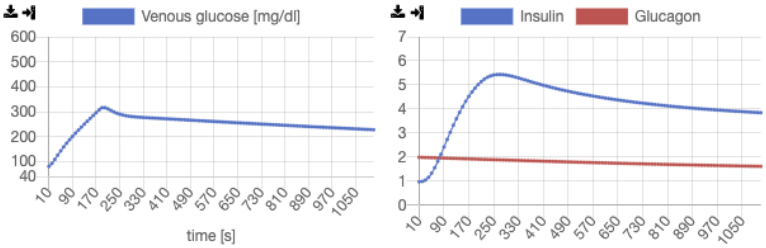

Some organs are sensitive to changes in glucose concentrations and their uptake of glucose
which have to be affected to deal with the glucose infusion are the liver and skeletal muscle.
the left side. The liver quickly stops producing glucose and intakes the first portion. The mus
right side you can see the glucose uptake for other tissues.

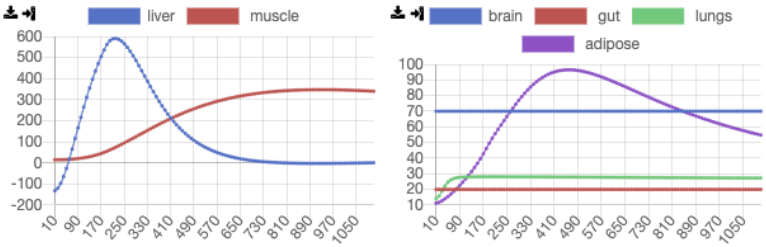

As you saw in the graphs before, the liver and the muscle are the most important to deal wit
glycogen breakdown and glycogen synthesis. In other words, less glucose gets produced and
liver (left) and the muscle (right) in the graphs below. Both flows are shown in mg/min.

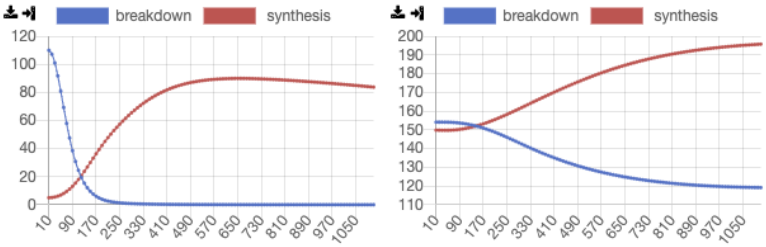

Figure 3.6: Web page section one graphs

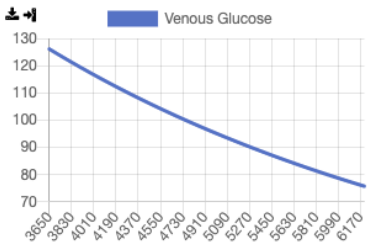

One of the tissues that are affected by insulin to uptake more glucose is the adipose tissue. Hov releases it as lacate. The process of converting glucose to lactate is called glycolysis. You can se outflow (more negative) of lactate.

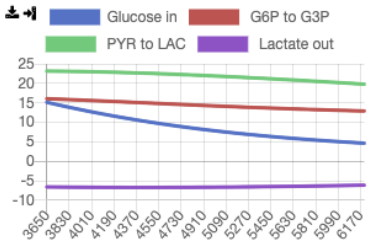

This extra lactate is one of the reasons for the increased lactate arterial levels.

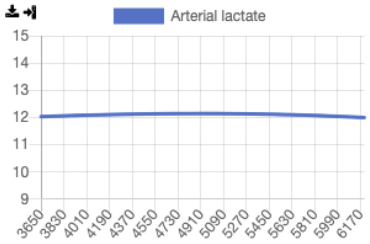

As described in the beggining, you can see that liver takes up more lactate. Some of this lactate

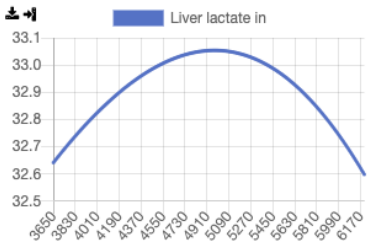

Figure 3.7: Web page section two graphs

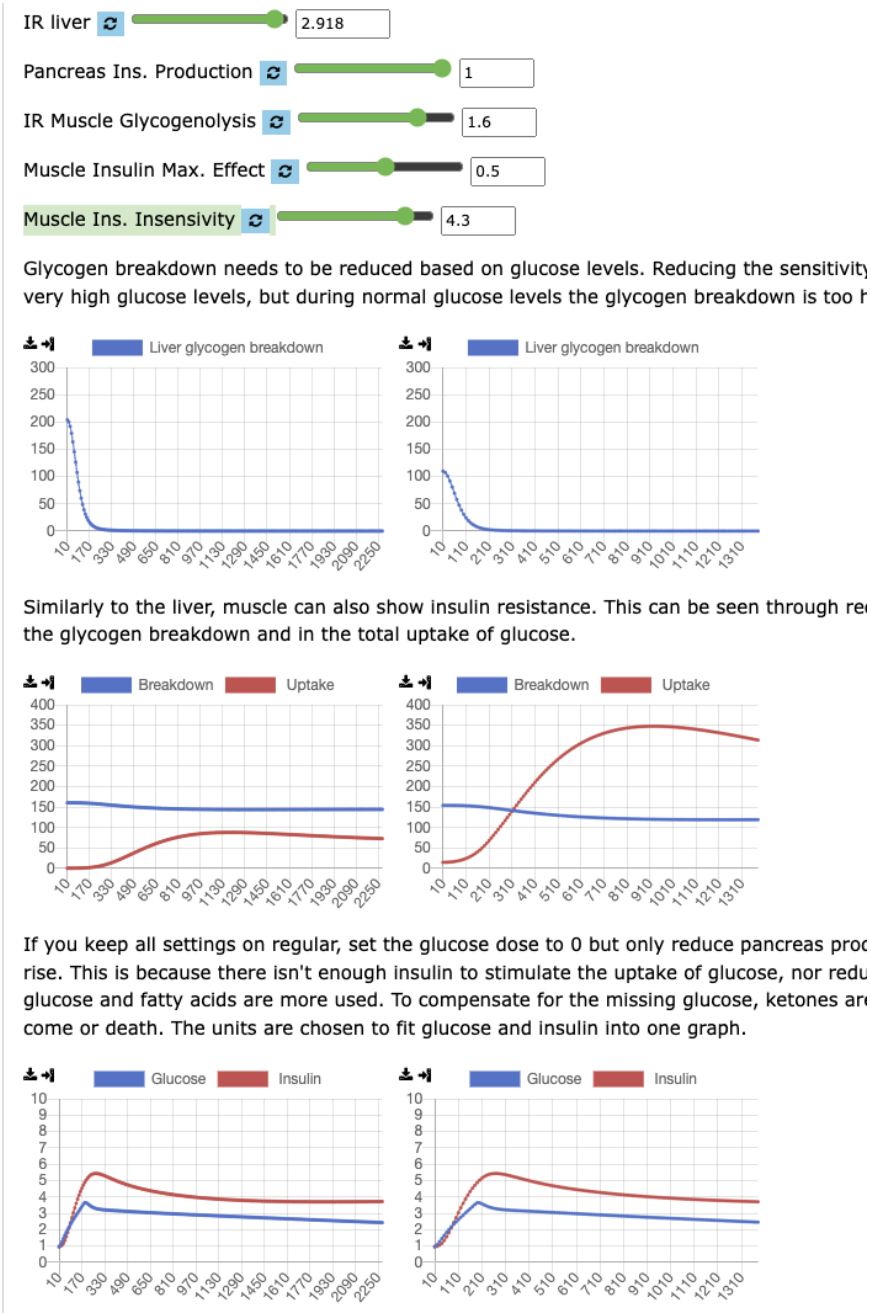

Figure 3.8: Web page section three graphs

Chapter 4

Conclusion

The objective of this thesis was to create a glucose metabolism model for educational purposes. The existing glucose metabolism models usually follow a minimalist approach to achieve their goals, which results in localized or only partially whole-body models. Although some models offer a great amount of detail, this detail is either localized to one particular tissue or makes the model very complex. In the first case, the models do not offer a full view of glucose metabolism. In the second case, the complex models require a lot of effort to understand which makes them less transparent and available for adaptations. This means that the current models' use in education is limited and was the source of the decision to produce a new model instead of using an existing one. The goal was to then use the educational model to display different points of view on glucose metabolism in an educational application - organ metabolite exchange, intracellular reactions, metabolite transformation, and regulation for homeostasis.

In order to fulfill the goal, several criteria were set as guidelines for the model. Firstly, to include all important tissues to close the loop of metabolite production and consumption in glucose metabolism. The organs/tissues devised to be modeled were: the brain, lungs, heart, liver, kidneys, skeletal muscle, adipose tissue, red blood cells, and gut. Secondly, to model important metabolites related to glucose metabolism, namely lactate, amino acids, and glycerol; with insulin and glucagon as regulators. Third, to contain intracellular reactions to the extent necessary to capture the process of glycogen breakdown, gluconeogenesis, and glycolysis. And at last, to join the tissues with a system of physical metabolite circulation. The model produced in this thesis matches all of the defined criteria.

The model builds primarily on the work of T. J. Sorensen[80] who developed a glucose metabolism model in his 1985 thesis. His model fulfills many of the goals stated in the paragraph above, namely a system of metabolite circulation, insulin and glucagon metabolism, and glucose dynamics for major organs. However, his model contains no intracellular reactions, combines some tissues, and treats them as one singular tissue. The combined tissues were modeled as separate in this model and their glucose metabolism was estimated. To model the processes not present in Sorensen's model, the work of Pratt et al.[71]

and Carstensen et al.[14] was used for the construction of an intracellular system of reactions. Using a modular approach, a general tissue object was created which was further adapted to form specific organs. This makes the model more simple to maintain and understand. Furthermore, it equalizes the depth of detail for different tissues and allows for straightforward comparison between organs. On the level of plasma metabolite concentration, the model reproduces qualitatively the data as published by Sorensen, although it is too sensitive to high insulin levels. The plasma metabolite values are produced by intracellular processes, in line with the existing theory.

The limitations of the model are that intracellular processes could be too simplified - for example in the kidney which has several different functional segments. The amino acid dynamics are constrained by not modeling individual amino acids, such as alanine and glutamine. There are several ways the model could be furthered. While the basal state is representative of glucose metabolism, expanding the model to represent exercise or food intake could offer new interesting simulations. The fatty acid metabolism is tightly connected to glucose metabolism and is affected for example in diabetes mellitus Type 2, which would add another layer of useful complexity to the model.

The web page is composed in line with the logic of showing different dimensions of glucose metabolism, as described in the section above, and is made of three sections. The first provides an overview of organ outflows and the process of glycogenolysis during a user-set intravenous glucose tolerance test. The second captures gluconeogenesis and glycolysis through lactate-glucose recycling. In the third, the user changes the metabolism's resistance to insulin and its capacity for insulin production to see how it affects the body's ability to achieve glucose homeostasis. These three sections should give the user a broad idea of how multi-faced glucose metabolism. The effect of the concept could be deepened by adding a point of view of several types of infusions; glucose, insulin, lactate, or combined glucose and insulin.

Besides creating the final products - the model and the web page - the process of writing this thesis also generated new information and byproducts that can contribute to further educational modeling of glucose metabolism. Namely, the glucose net uptake basal rates for the newly added tissues, the estimated new blood flows and volumes for the muscle and adipose tissue, and the programmed Modelica objects.

Bibliography

[1] ABDUL KADIR, Azrul, Kieran CLARKE, and Rhys D. EVANS. Cardiac ketone body metabolism. *Biochimica et Biophysica Acta (BBA) - Molecular Basis of Disease* [online]. 2020, **1866**(6), 165739 [viewed 4 January 2023]. ISSN 0925-4439. Available from: doi:10.1016/j.bbadis.2020.165739

[2] ADEVA-ANDANY, María M., et al. Liver glucose metabolism in humans. *Bioscience Reports* [online]. 2016, **36**(6) [viewed 13 December 2022]. ISSN 1573-4935. Available from: doi:10.1042/bsr20160385

[3] AISTON, S., B. ANDERSEN, and L. AGIUS. Glucose 6-phosphate regulates hepatic glycogenolysis through inactivation of phosphorylase. *Diabetes* [online]. 2003, **52**(6), 1333–1339 [viewed 12 December 2022]. ISSN 1939-327X. Available from: doi:10.2337/diabetes.52.6.1333

[4] AJMERA, I., et al. The impact of mathematical modeling on the understanding of diabetes and related complications. *CPT: Pharmacometrics & Systems Pharmacology* [online]. 2013, **2**(7), 54. ISSN 2163-8306 [viewed 13 September 2022]. Available from: doi:10.1038/psp.2013.30

[5] ALVEHAG, Karin, and Clyde MARTIN. The Feedback Control of Glucose: On the road to type II diabetes. In: *Proceedings of the 45th IEEE conference on decision and control* [online]. IEEE, 2006. ISBN 1424401712 [viewed 13 September 2022]. Available from: doi:10.1109/cdc.2006.377192

[6] ALVES-BEZZERA, Michele, and David E. Cohen. Triglyceride metabolism in the liver. *Comprehensive Physiology* [online]. 2017, **8**(1), 1-8 [viewed 12 December 2022]. ISSN 2040-4603. Available from: doi:10.1002/cphy.c170012

[7] ANDRÉS-VILLARREAL, Mireia, et al. Measuring water distribution in the heart: preventing edema reduces ischemia–reperfusion injury. *Journal of the American Heart Association* [online]. 2016, **5**(12) [viewed 19 December 2022]. ISSN 2047-9980. Available from: doi:10.1161/jaha.116.003843

[8] DOMINICZAK, Marek H., and John W. BAYNES. *Medical biochemistry*. 2nd ed. Mosby, 2004. ISBN 9780723433415.

[9] BERGMAN, R. N., et al. Quantitative estimation of insulin sensitivity. *American Journal of Physiology-Endocrinology and Metabolism* [online]. 1979, **236**(6), E667. ISSN 1522-1555 [viewed 13 September 2022]. Available from: doi:10.1152/ajpendo.1979.236.6.e667

[10] BLANCO, Antonio, and Gustavo BLANCO. Integration and regulation of metabolism. In: *Medical biochemistry* [online]. Elsevier, 2017, pp. 425–445 [viewed 9 January 2023]. ISBN 9780128035504. Available from: doi:10.1016/b978-0-12-803550-4.00019-7

[11] BROOKS, George A. Lactate as a fulcrum of metabolism. *Redox Biology* [online]. 2020, **35**, 101454 [viewed 20 December 2022]. ISSN 2213-2317. Available from: doi:10.1016/j.redox.2020.101454

[12] BUSTOS, Diego M., and Alberto A. IGLESIAS. The kinetic properties of liver glucokinase and its function in glucose physiology as a model for the comprehensive study of enzymes' kinetic parameters and reversible inhibitors. *Biochemistry and Molecular Biology Education* [online]. 2000, **28**(6), 332–337 [viewed 12 December 2022]. ISSN 1539-3429. Available from: doi:10.1111/j.1539-3429.2000.tb00186.x

[13] CARLSEN, Anders, and Jens Otto WIETH. Glycerol transport in human red cells. *Acta Physiologica Scandinavica* [online]. 1976, **97**(4), 501–513 [viewed 20 December 2022]. ISSN 1365-201X. Available from: doi:10.1111/j.1748-1716.1976.tb10290.x

[14] CARSTENSEN, Peter Emil et al. A whole-body multi-scale mathematical model for dynamic simulation of the metabolism in man. Biorxiv [online]. 2022. [viewed 15 September 2022]. Available from: https://arxiv.org/pdf/2205.01473.pdf

[15] CARTA, Gianfranca, et al. Palmitic acid: physiological role, metabolism and nutritional implications. *Frontiers in Physiology* [online]. 2017, **8** [viewed 14 December 2022]. ISSN 1664-042X. Available from: doi:10.3389/fphys.2017.00902

[16] CERSOSIMO, Eugenio, Peter GARLICK, and John FERRETTI. Insulin regulation of renal glucose metabolism in humans. *American Journal of Physiology-Endocrinology and Metabolism* [online]. 1999, **276**(1), E78—E84 [viewed 3 January 2023]. ISSN 1522-1555. Available from: doi:10.1152/ajpendo.1999.276.1.e78

[17] CULLEN, Kirsty S., et al. Glucagon induces translocation of glucokinase from the cytoplasm to the nucleus of hepatocytes by transfer between 6-phosphofructo 2-kinase/fructose 2,6-bisphosphatase-2 and the glucokinase regulatory protein. *Biochimica et Biophysica Acta (BBA) - Molecular Cell Research* [online]. 2014, **1843**(6),

1123–1134 [viewed 14 December 2022]. ISSN 0167-4889. Available from: doi:10.1016/j.bbamcr.2014.02.006

[18] DALLA MAN, Chiara, Robert A. RIZZA, and Claudio COBELLI. Meal Simulation Model of the Glucose-Insulin System. *IEEE Transactions on Biomedical Engineering* [online]. 2007, **54**(10), 1740–1749. ISSN 0018-9294 [viewed 13 September 2022]. Available from: doi:10.1109/tbme.2007.893506

[19] DEROUICH, M., and A. BOUTAYEB. The effect of physical exercise on the dynamics of glucose and insulin. *Journal of Biomechanics* [online]. 2002, **35**(7), 911–917. ISSN 0021-9290 [viewed 13 September 2022]. Available from: doi:10.1016/s0021-9290(02)00055-6

[20] DIENEL, Gerald A. Brain glucose metabolism: integration of energetics with function. *Physiological Reviews* [online]. 2019, **99**(1), 949–1045 [viewed 11 December 2022]. ISSN 1522-1210. Available from: doi:10.1152/physrev.00062.2017

[21] DIMITRIADIS, George, et al. Insulin effects in muscle and adipose tissue. *Diabetes Research and Clinical Practice* [online]. 2011, **93**, S52—S59 [viewed 14 December 2022]. ISSN 0168-8227. Available from: doi:10.1016/s0168-8227(11)70014-6

[22] EDGERTON, D. S. Insulin's direct effects on the liver dominate the control of hepatic glucose production. *Journal of Clinical Investigation* [online]. 2006, **116**(2), 521–527 [viewed 13 December 2022]. ISSN 0021-9738. Available from: doi:10.1172/jci27073

[23] ERLANDSEN, Mogens, Christoffer MARTINUSSEN, and Claus Højbjerg GRAVHOLT. Integrated model of insulin and glucose kinetics describing both hepatic glucose and pancreatic insulin regulation. *Computer Methods and Programs in Biomedicine* [online]. 2018, **156**, 121–131. ISSN 0169-2607 [viewed 13 September 2022]. Available from: doi:10.1016/j.cmpb.2017.12.009

[24] EVANS, Mark, Karl E. COGAN, and Brendan EGAN. Metabolism of ketone bodies during exercise and training: physiological basis for exogenous supplementation. *The Journal of Physiology* [online]. 2016, **595**(9), 2857–2871 [viewed 14 December 2022]. ISSN 0022-3751. Available from: doi:10.1113/jp273185

[25] FRAYN, Keith N., Sandy M. HUMPHREYS, and Simon W. COPPACK. Fuel selection in white adipose tissue. *Proceedings of the Nutrition Society* [online]. 1995, **54**(1), 177–189 [viewed 22 December 2022]. ISSN 1475-2719. Available from: doi:10.1079/pns19950047

[26] FRAYN, Keith N., Peter ARNER, and Hannele YKI-JÄRVINEN. Fatty acid metabolism in adipose tissue, muscle and liver in health and disease.

Essays in Biochemistry [online]. 2006, *42*, 89–103 [viewed 14 December 2022]. ISSN 1744-1358. Available from: doi:10.1042/bse0420089

[27] GALICIA-GARCIA, Unai, et al. Pathophysiology of type 2 diabetes mellitus. *International Journal of Molecular Sciences* [online]. 2020, **21**(17), 6275 [viewed 15 December 2022]. ISSN 1422-0067. Available from: doi:10.3390/ijms21176275

[28] GASTALDELLI, A., et al. Effect of physiological hyperinsulinemia on gluconeogenesis in nondiabetic subjects and in type 2 diabetic patients. *Diabetes* [online]. 2001, **50**(8), 1807–1812 [viewed 14 December 2022]. ISSN 1939-327X. Available from: doi:10.2337/diabetes.50.8.1807

[29] GORESKY, Carl A., et al. Uptake of lactate by the liver: effect of red blood cell carriage. *American Journal of Physiology-Gastrointestinal and Liver Physiology* [online]. 2000, **278**(5), G775—G788 [viewed 20 December 2022]. ISSN 1522-1547. Available from: doi:10.1152/ajpgi.2000.278.5.g775

[30] GUARINO, Victoria A., et al. Reaction rate of pyruvate and hydrogen peroxide: assessing antioxidant capacity of pyruvate under biological conditions. *Scientific Reports* [online]. 2019, **9**(1) [viewed 20 December 2022]. ISSN 2045-2322. Available from: doi:10.1038/s41598-019-55951-9

[31] HACKNEY, Kyle J., et al. Skeletal muscle volume following dehydration induced by exercise in heat. *Extreme Physiology & Medicine* [online]. 2012, **1**(1), 3 [viewed 19 December 2022]. ISSN 2046-7648. Available from: doi:10.1186/2046-7648-1-3

[32] HAN, Hye-Sook, et al. Regulation of glucose metabolism from a liver-centric perspective. *Experimental & Molecular Medicine* [online]. 2016, **48**(3), e218-e218 [viewed 13 December 2022]. ISSN 2092-6413. Available from: doi:10.1038/emm.2015.122

[33] HATTING, Maximilian, et al. Insulin regulation of gluconeogenesis. *Annals of the New York Academy of Sciences* [online]. 2017, **1411**(1), 21–35 [viewed 12 December 2022]. ISSN 0077-8923. Available from: doi:10.1111/nyas.13435

[34] HAVEL, R. J., et al. Splanchnic metabolism of free fatty acids and production of triglycerides of very low density lipoproteins in normotriglyceridemic and hypertriglyceridemic humans. *Journal of Clinical Investigation* [online]. 1970, **49**(11), 2017–2035 [viewed 3 January 2023]. ISSN 0021-9738. Available from: doi:10.1172/jci106422

[35] HEINONEN, Ilkka, et al. Bone blood flow and metabolism in humans: effect of muscular exercise and other physiological perturbations. *Journal of Bone and Mineral Research* [online]. 2013, **28**(5), 1068–1074 [viewed 20 December 2022]. ISSN 0884-0431. Available from: doi:10.1002/jbmr.1833

[36] HERRGÅRDH, Tilda, et al. An updated organ-based multi-level model for glucose homeostasis: organ distributions, timing, and impact of blood flow. *Frontiers in Physiology* [online]. 2021, **12**. ISSN 1664-042X [viewed 14 September 2022]. Available from: doi:10.3389/fphys.2021.619254

[37] ICHAI, Carole, et al. Glucose 6-phosphate hydrolysis is activated by glucagon in a low temperature-sensitive manner. *Journal of Biological Chemistry* [online]. 2001, **276**(30), 28126–28133 [viewed 3 January 2023]. ISSN 1083-351X. Available from: doi:10.1074/jbc.m010186200

[38] ILIADIS, Fotios, Nikolaos KADOGLOU, and Triantafillos DIDANGELOS. Insulin and the heart. *Diabetes Research and Clinical Practice* [online]. 2011, **93**, S86—S91 [viewed 22 December 2022]. ISSN 0168-8227. Available from: doi:10.1016/s0168-8227(11)70019-5

[39] ROSE, Irwin A., and Jessie V. B. WARMS. Control of glycolysis in the human red blood cell. *Journal of Biological Chemistry* [online]. 1966, **241**(21), 4848–4854 [viewed 3 January 2023]. ISSN 0021-9258. Available from: doi:10.1016/s0021-9258(18)99643-2

[40] JANSSEN, Ian, et al. Skeletal muscle mass and distribution in 468 men and women aged 18–88 yr. *Journal of Applied Physiology* [online]. 2000, **89**(1), 81–88 [viewed 14 December 2022]. ISSN 1522-1601. Available from: doi:10.1152/jappl.2000.89.1.81

[41] JOYNER, Michael J., et al. Sympathetic nerves and control of blood vessels to human limbs. In: Peripheral neuropathy [online]. Elsevier, 2005, pp. 323–337 [viewed 20 December 2022]. ISBN 9780721694917. Available from: doi:10.1016/b978-0-7216-9491-7.50018-1

[42] KAMATA, Kenji, et al. Structural basis for allosteric regulation of the monomeric allosteric enzyme human glucokinase. *Structure* [online]. 2004, **12**(3), 429–438 [viewed 12 December 2022]. ISSN 0969-2126. Available from: doi:10.1016/j.str.2004.02.005

[43] PAUL F. KANTOR, GARY D. LOPASCHUK, LIONEL H. OPIE, CHAPTER 32 - Myocardial Energy Metabolism, Editor(s): NICHOLAS SPERELAKIS, YOSHIHISA KURACHI, ANDRE TERZIC, MICHAEL V. COHEN, Heart Physiology and Pathophysiology (Fourth Edition), *Academic Press*, 2001, Pages 543-569, ISBN 9780126569759. Available from: doi.org/10.1016/B978-012656975-9/50034-1

[44] KELLEY, D., et al. Skeletal muscle glycolysis, oxidation, and storage of an oral glucose load. *Journal of Clinical Investigation* [online]. 1988, **81**(5), 1563–1571 [viewed 14 December 2022]. ISSN 0021-9738. Available from: doi:10.1172/jci113489

[45] KELLEY, D. E., et al. Effects of insulin on skeletal muscle glucose storage, oxidation, and glycolysis in humans. *American Journal*

of Physiology-Endocrinology and Metabolism [online]. 1990, **258**(6), E923—E929 [viewed 22 December 2022]. ISSN 1522-1555. Available from: doi:10.1152/ajpendo.1990.258.6.e923

[46] KHAN, Moien Abdul Basith, et al. Epidemiology of type 2 diabetes – global burden of disease and forecasted trends. *Journal of Epidemiology and Global Health* [online]. 2019, **10**(1), 107 [viewed 10 January 2023]. ISSN 2210-6014. Available from: doi:10.2991/jegh.k.191028.001

[47] KRAEGEN, E. W., et al. Dose-response curves for in vivo insulin sensitivity in individual tissues in rats. *American Journal of Physiology-Endocrinology and Metabolism* [online]. 1985, **248**(3), E353—E362 [viewed 9 January 2023]. ISSN 1522-1555. Available from: doi:10.1152/ajpendo.1985.248.3.e353

[48] KRYCER, James R., et al. Lactate production is a prioritized feature of adipocyte metabolism. *Journal of Biological Chemistry* [online]. 2019, **295**(1), 83–98 [viewed 22 December 2022]. ISSN 1083-351X. Available from: doi:10.1074/jbc.ra119.011178

[49] KURATA, Hiroyuki. Virtual metabolic human dynamic model for pathological analysis and therapy design for diabetes. *iScience* [online]. 2021, **24**(2), 102101. ISSN 2589-0042 [viewed 14 September 2022]. Available from: doi:10.1016/j.isci.2021.102101

[50] LAFONTAN, M. Advances in adipose tissue metabolism. *International Journal of Obesity* [online]. 2008, **32**(S7), S39—S51 [viewed 22 December 2022]. ISSN 1476-5497. Available from: doi:10.1038/ijo.2008.237

[51] LEGOUIS, David, et al. Renal gluconeogenesis: an underestimated role of the kidney in systemic glucose metabolism. *Nephrology Dialysis Transplantation* [online]. 2020 [viewed 22 December 2022]. ISSN 1460-2385. Available from: doi:10.1093/ndt/gfaa302

[52] LEIDER, Morris. On the weight of the skin. *Journal of Investigative Dermatology* [online]. 1949, **12**(3), 187–191 [viewed 20 December 2022]. ISSN 0022-202X. Available from: doi:10.1038/jid.1949.28

[53] LI, Xue-bing, Jun-dong GU, and Qing-hua ZHOU. Review of aerobic glycolysis and its key enzymes - new targets for lung cancer therapy. *Thoracic Cancer* [online]. 2015, **6**(1), 17–24 [viewed 6 January 2023]. ISSN 1759-7706. Available from: doi:10.1111/1759-7714.12148

[54] LIU, Weijiu, and Fusheng TANG. Modeling a simplified regulatory system of blood glucose at molecular levels. *Journal of Theoretical Biology*[online]. 2008, **252**(4), 608–620. ISSN 0022-5193 [viewed 13 September 2022]. Available from: doi:10.1016/j.jtbi.2008.02.021

[55] LIONETTI, V., W. C. STANLEY, and F. A. RECCHIA. Modulating fatty acid oxidation in heart failure. *Cardiovascular Research* [online].

2011, **90**(2), 202–209 [viewed 14 December 2022]. ISSN 0008-6363. Available from: doi:10.1093/cvr/cvr038

[56] MERGENTHALER, Philipp, et al. Sugar for the brain: the role of glucose in physiological and pathological brain function. *Trends in Neurosciences* [online]. 2013, **36**(10), 587–597 [viewed 11 December 2022]. ISSN 0166-2236. Available from: doi:10.1016/j.tins.2013.07.001

[57] MEYER, Christian, et al. Effects of physiological hyperinsulinemia on systemic, renal, and hepatic substrate metabolism. *American Journal of Physiology-Renal Physiology*[online]. 1998, **275**(6), F915—F921 [viewed 14 December 2022]. ISSN 1522-1466. Available from: doi:10.1152/ajprenal.1998.275.6.f915

[58] MEYER, Christian, et al. Role of human liver, kidney, and skeletal muscle in postprandial glucose homeostasis. *American Journal of Physiology-Endocrinology and Metabolism* [online]. 2002, **282**(2), E419—E427 [viewed 14 December 2022]. ISSN 1522-1555. Available from: doi:10.1152/ajpendo.00032.2001

[59] MITCHELL, H. H., et al. The chemical composition of the adult human body and its bearing on the biochemistry of growth. *Journal of Biological Chemistry* [online]. 1945, **158**(3), 625–637 [viewed 19 December 2022]. ISSN 0021-9258. Available from: doi:10.1016/s0021-9258(19)51339-4

[60] MITHIEUX, Gilles. New data and concepts on glutamine and glucose metabolism in the gut. *Current Opinion in Clinical Nutrition and Metabolic Care* [online]. 2001, **4**(4), 267–271 [viewed 22 December 2022]. ISSN 1363-1950. Available from: doi:10.1097/00075197-200107000-00004

[61] MITROU, Panayota, et al. Rates of glucose uptake in adipose tissue and musclein vivoafter a mixed meal in women with morbid obesity. *The Journal of Clinical Endocrinology & Metabolism* [online]. 2009, **94**(8), 2958–2961 [viewed 22 December 2022]. ISSN 1945-7197. Available from: doi:10.1210/jc.2008-2297

[62] MOBERG, Erik, et al. No apparent suppression by insulin of in vivo skeletal muscle lipolysis in nonobese women. *American Journal of Physiology-Endocrinology and Metabolism* [online]. 2002, **283**(2), E295—E301 [viewed 22 December 2022]. ISSN 1522-1555. Available from: doi:10.1152/ajpendo.00339.2001

[63] MOLINA, D. Kimberley, and Vincent J. M. DIMAIO. Normal organ weights in men. *The American Journal of Forensic Medicine and Pathology* [online]. 2012, **33**(4), 368–372 [viewed 22 December 2022]. ISSN 0195-7910. Available from: doi:10.1097/paf.0b013e31823d29ad

[64] MOTYL, Katherine J., et al. Energy metabolism of bone. *Toxicologic Pathology* [online]. 2017, **45**(7), 887–893 [viewed 19 December 2022]. ISSN 1533-1601. Available from: doi:10.1177/0192623317737065

[65] NGUYEN, D. T., and D. KEAST. Energy metabolism and the skin. *International Journal of Biochemistry* [online]. 1991, **23**(11), 1175–1183 [viewed 20 December 2022]. ISSN 0020-711X. Available from: doi:10.1016/0020-711x(91)90213-7

[66] NYMAN, Elin, et al. A hierarchical whole-body modeling approach elucidates the link between in vitro insulin signaling and in vivo glucose homeostasis. *Journal of Biological Chemistry* [online]. 2011, **286**(29), 26028–26041. ISSN 1083-351X [viewed 14 September 2022]. Available from: doi:10.1074/jbc.m110.188987

[67] OIKONEN, Vesa. TPC - Adipose tissue. *Analysis of PET studies* [online]. 3 January 2022 [viewed 19 December 2022]. Available from: http://www.turkupetcentre.net/petanalysis/organ_wat.html

[68] O'NEIL, J.J., and D.F. TIERNEY. Rat lung metabolism: glucose utilization by isolated perfused lungs and tissue slices. *American Journal of Physiology-Legacy Content* [online]. 1974, **226**(4), 867–873 [viewed 22 December 2022]. ISSN 0002-9513. Available from: doi:10.1152/ajplegacy.1974.226.4.867

[69] PANUNZI, Simona, et al. A revised Sorensen model: simulating glycemic and insulinemic response to oral and intra-venous glucose load. *PLOS ONE* [online]. 2020, **15**(8), e0237215 [viewed 12 December 2022]. ISSN 1932-6203. Available from: doi:10.1371/journal.pone.0237215

[70] PAGLIALUNGA, Sabina, and Clayton A. DEHN. Clinical assessment of hepatic de novo lipogenesis in non-alcoholic fatty liver disease. *Lipids in Health and Disease* [online]. 2016, **15**(1) [viewed 3 January 2023]. ISSN 1476-511X. Available from: doi:10.1186/s12944-016-0321-5

[71] PRATT, Adrian C., Jonathan A. D. WATTIS, and Andrew M. SALTER. Mathematical modeling of hepatic lipid metabolism. *Mathematical Biosciences* [online]. 2015, **262**, 167–181. ISSN 0025-5564 [viewed 14 September 2022]. Available from: doi:10.1016/j.mbs.2014.12.012

[72] RAMNANAN, C. J., et al. Physiologic action of glucagon on liver glucose metabolism. *Diabetes, Obesity and Metabolism* [online]. 2011, **13**, 118–125 [viewed 14 December 2022]. ISSN 1462-8902. Available from: doi:10.1111/j.1463-1326.2011.01454.x

[73] ROSS, Brian D., Joseph ESPINAL, and Patricio SILVA. Glucose metabolism in renal tubular function. *Kidney International*[online]. 1986, **29**(1), 54–67 [viewed 22 December 2022]. ISSN 0085-2538. Available from: doi:10.1038/ki.1986.8

[74] SCHALLER, S., et al. A generic integrated physiologically based whole-body model of the glucose-insulin-glucagon regulatory system. *CPT: Pharmacometrics & Systems Pharmacology* [online]. 2013, **2**(8), 65. ISSN 2163-8306 [viewed 14 September 2022]. Available from: doi:10.1038/psp.2013.40

[75] SASAKI, Motohiro, et al. Dual regulation of gluconeogenesis by insulin and glucose in the proximal tubules of the kidney. *Diabetes* [online]. 2017, **66**(9), 2339–2350 [viewed 22 December 2022]. ISSN 1939-327X. Available from: doi:10.2337/db16-1602

[76] ŠILAR, Jan, et al. Development of in-browser simulators for medical education: introduction of a novel software toolchain. *Journal of Medical Internet Research* [online]. 2019, **21**(7), e14160 [viewed 19 December 2022]. ISSN 1438-8871. Available from: doi:10.2196/14160

[77] SILBER, Hanna E., et al. An integrated model for glucose and insulin regulation in healthy volunteers and type 2 diabetic patients following intravenous glucose provocations. *The Journal of Clinical Pharmacology* [online]. 2007, **47**(9), 1159–1171. ISSN 0091-2700 [viewed 13 September 2022]. Available from: doi:10.1177/0091270007304457

[78] SILBER, Hanna E., Nicolas FREY, and Mats O. KARLSSON. An integrated glucose-insulin model to describe oral glucose tolerance test data in healthy volunteers. *The Journal of Clinical Pharmacology* [online]. 2010, **50**(3), 246–256. ISSN 0091-2700 [viewed 13 September 2022]. Available from: doi:10.1177/0091270009341185

[79] SILVERTHORN, Dee Unglaub. *Human physiology: an integrated approach.* 6th ed. Boston: Pearson Education, 2013. ISBN 9780321750075.

[80] SORENSEN, John Thomas. A physiologic model of glucose metabolism in man and its use to design and assess improved insulin therapies for diabetes. PhD diss., Massachusetts Institute of Technology, 1985.

[81] STANLEY, J. C., et al. Activities of glucokinase and hexokinase in mammalian and avian livers.*Biochemical Journal* [online]. 1984, **224**(2), 667–671 [viewed 12 December 2022]. ISSN 1470-8728. Available from: doi:10.1042/bj2240667

[82] STANLEY, William C., and Margaret P. CHANDLER. *Heart Failure Reviews* [online]. 2002, **7**(2), 115–130 [viewed 3 January 2023]. ISSN 1382-4147. Available from: doi:10.1023/a:1015320423577

[83] TOGHAW, Puntip, et al. Bariatric surgery and T2DM improvement mechanisms: a mathematical model. *Theoretical Biology and Medical modeling* [online]. 2012, **9**(1), 16. ISSN 1742-4682 [viewed 13 September 2022]. Available from: doi:10.1186/1742-4682-9-16

[84] TUNNICLIFF, G. Amino acid transport by human erythrocyte membranes. *Comparative Biochemistry and Physiology Part A: Physiology* [online]. 1994, **108**(4), 471–478 [viewed 6 January 2023]. ISSN 0300-9629. Available from: doi:10.1016/0300-9629(94)90329-8

[85] ULUSEKER, Cansu, et al. A closed-loop multi-level model of glucose homeostasis. *PLOS ONE* [online]. 2018, **13**(2), e0190627. ISSN 1932-6203 [viewed 14 September 2022]. Available from: doi:10.1371/journal.pone.0190627

[86] URETA, Tito, Pedro A. LAZO, and Alberto SOLS. Allosteric inhibition of brain hexokinase by glucose 6-phosphate in the reverse reaction. *Archives of Biochemistry and Biophysics* [online]. 1985, **239**(2), 315–319 [viewed 14 December 2022]. ISSN 0003-9861. Available from: doi:10.1016/0003-9861(85)90693-9

[87] VAHIDI, O., et al. A comprehensive compartmental model of blood glucose regulation for healthy and type 2 diabetic subjects. *Medical & Biological Engineering & Computing* [online]. 2015, **54**(9), 1383–1398. ISSN 1741-0444 [viewed 15 September 2022]. Available from: doi:10.1007/s11517-015-1406-4

[88] VAN HALL, G., et al. Human skeletal muscle fatty acid and glycerol metabolism during rest, exercise and recovery. *The Journal of Physiology* [online]. 2002, **543**(3), 1047–1058 [viewed 14 December 2022]. ISSN 1469-7793. Available from: doi:10.1113/jphysiol.2002.023796

[89] VAN HALL, Gerrit. Lactate kinetics in human tissues at rest and during exercise. *Acta Physiologica* [online]. 2010, **199**(4), 499–508 [viewed 14 December 2022]. ISSN 1748-1708. Available from: doi:10.1111/j.1748-1716.2010.02122.x

[90] VAN SCHAFTINGEN, Emile, and Isabelle GERIN. The glucose-6-phosphatase system. *Biochemical Journal* [online]. 2002, **362**(3), 513 [viewed 12 December 2022]. ISSN 0264-6021. Available from: doi:10.1042/0264-6021:3620513

[91] VIRTANEN, Kirsi A., et al. Glucose uptake and perfusion in subcutaneous and visceral adipose tissue during insulin stimulation in nonobese and obese humans. *The Journal of Clinical Endocrinology & Metabolism* [online]. 2002, **87**(8), 3902–3910 [viewed 14 December 2022]. ISSN 1945-7197. Available from: doi:10.1210/jcem.87.8.8761

[92] VISENTIN, Roberto, et al. The uva/padova type 1 diabetes simulator goes from single meal to single day. *Journal of Diabetes Science and Technology* [online]. 2018, **12**(2), 273–281. ISSN 1932-2968 [viewed 13 September 2022]. Available from: doi:10.1177/1932296818757747

[93] VILLAR-PALASÍ, Carlos, and Joan J. GUINOVART. The role of glucose 6-phosphate in the control of glycogen synthase. *The FASEB*

Journal [online]. 1997, **11**(7), 544–558 [viewed 12 December 2022]. ISSN 1530-6860. Available from: doi:10.1096/fasebj.11.7.9212078

[94] XU, Ke, et al. A whole-body model for glycogen regulation reveals a critical role for substrate cycling in maintaining blood glucose homeostasis. *PLoS Computational Biology* [online]. 2011, **7**(12), e1002272. ISSN 1553-7358 [viewed 14 September 2022]. Available from: doi:10.1371/journal.pcbi.1002272

[95] WOLFE, R. R., et al. Role of triglyceride-fatty acid cycle in controlling fat metabolism in humans during and after exercise. *American Journal of Physiology-Endocrinology and Metabolism* [online]. 1990, **258**(2), E382—E389 [viewed 3 January 2023]. ISSN 1522-1555. Available from: doi:10.1152/ajpendo.1990.258.2.e382

[96] WANG, ZiMian, et al. Specific metabolic rates of major organs and tissues across adulthood: evaluation by mechanistic model of resting energy expenditure. *The American Journal of Clinical Nutrition* [online]. 2010, **92**(6), 1369–1377 [viewed 14 December 2022]. ISSN 1938-3207. Available from: doi:10.3945/ajcn.2010.29885

[97] WASIK, Anita A., and Sanna LEHTONEN. Glucose transporters in diabetic kidney disease—friends or foes? *Frontiers in Endocrinology* [online]. 2018, **9** [viewed 22 December 2022]. ISSN 1664-2392. Available from: doi:10.3389/fendo.2018.00155

[98] ZHANG, Xueping, et al. Unraveling the regulation of hepatic gluconeogenesis. *Frontiers in Endocrinology* [online]. 2019, **9** [viewed 6 January 2023]. ISSN 1664-2392. Available from: doi:10.3389/fendo.2018.00802